

---

# Taming Generative Diffusion Prior for Universal Blind Image Restoration

---

Siwei Tu<sup>1</sup>, Weidong Yang<sup>1,†</sup>, Ben Fei<sup>2,†</sup>

<sup>1</sup>Fudan University, <sup>2</sup>Chinese University of Hong Kong

24110240079@m.fudan.edu.cn, wdyang@fudan.edu.cn, benfei@cuhk.edu.hk

† Corresponding Authors

## Abstract

Diffusion models have been widely utilized for image restoration. However, previous blind image restoration methods still need to assume the type of degradation model while leaving the parameters to be optimized, limiting their real-world applications. Therefore, we aim to tame generative diffusion prior for universal blind image restoration dubbed **BIR-D**, which utilizes an **optimizable convolutional kernel** to simulate the degradation model and dynamically update the parameters of the kernel in the diffusion steps, enabling it to achieve blind image restoration results even in various complex situations. Besides, based on mathematical reasoning, we have provided an empirical formula for the chosen of **adaptive guidance scale**, eliminating the need for a grid search for the optimal parameter. Experimentally, Our BIR-D has demonstrated superior practicality and versatility than off-the-shelf unsupervised methods across various tasks both on real-world and synthetic datasets, qualitatively and quantitatively. BIR-D is able to fulfill multi-guidance blind image restoration. Moreover, BIR-D can also restore images that undergo multiple and complicated degradations, demonstrating the practical applications. The code is available at <https://github.com/Tusiwei/BIR-D>

## 1 Introduction



Figure 1: Blind Image Restoration Diffusion Model (BIR-D) can achieve high-quality restoration for different types of degraded images. BIR-D not only has the capability to restore (a) linear inverse problems when the degradation function is known. BIR-D can also achieve high-quality image restoration in (b) blind issues with unknown degradation functions, as well as in (c) mixed degradation and real degradation scenarios.

Images inevitably suffer from a degradation in quality in the process of capturing, storing, and compressing. Thus, the image restoration task intends to establish a mapping between the degraded image and the original image, to recover a high-quality image from the degraded image. In an ideal scenario, the ultimate goal is to undo and restore the degradation process of the image. However, in reality, the complexity of the degradation mode often leads to the incapability to fully restore the original high-quality image, which also makes traditional supervised approaches unsuitable for all types of image restoration tasks. According to the degradation mode, image restoration tasks can be divided into two types: **non-blind** and **blind** problems. **Blind** problems, such as low light enhancement, motion blur reduction and HDR image restoration, refer to image restoration problems where the degradation functions and parameters are totally unknown.

The blind image restoration problem has attracted increasing attention with the development of generative models. The unsupervised blind image restoration methods represented by Generative Adversarial Networks (GANs) [1; 2; 3; 4] have the capability to train networks on large datasets of clean images and learn real-world knowledge. However, GANs are still difficult to avoid falling into limitations such as poor diversity and difficulty in model training. In parallel, diffusion model [5; 6; 7; 8; 9] have shown strong performance in terms of quality and diversity compared to GANs. Pioneer works such as GDP [10], DDRM [11], and DDNM [12] attempt to solve such problems by incorporating the degraded image  $y$  as guidance in the sampling process of diffusion models. By modeling posterior distributions in an unsupervised sampling manner, these approaches showcase the potential for practical guidance in blind image restoration, offering promising implications for real-world applications. However, the degradation types in these models still need to be assumed, limiting the practicality of natural image restoration where the complicated degradation models always remain unknown.

To this end, we propose an effective and versatile Blind Image Restoration Diffusion Model (BIR-D). It utilizes well-trained DDPM [13] as an effective prior and is guided by degraded images to form a universal method for various image restoration and enhancement tasks. To uniformly model the unknown degradation function of blind image restoration, an optimizable convolutional kernel is dynamically optimized and utilized to simulate the degradation function at each denoising step. Specifically, BIR-D updates the convolution kernel parameters based on the gradient of distance loss between the generated image undergoing our optimizable convolutional kernel and the given degraded image. At the same time, all existing image restoration methods [10; 11; 12] that use diffusion models manually set the guidance scale as a hyperparameter to control the magnitude of guided generation, which also remains unchanged throughout the sampling process. However, for images from different tasks, the guidance scale required for each diffusion step is not entirely the same. To deal with this issue, we have derived an empirical formula for the guidance scale, which can calculate the optimal guidance scale for the next denoising step in real-time during the sampling process. This improvement avoids the need to manually grid search the optimal value of the guidance scale when solving different tasks and also enhances the quality of generated images. With the help of a well-trained DDPM, the above designs enable BIR-D to tackle various blind image restoration tasks. BIR-D can also achieve multi-degradation or multi-guidance image restoration. Furthermore, it showcases satisfactory results in addressing restoration issues related to complex degradation types encountered in real-world scenarios.

## 2 BIR-D: Universal Blind Image Restoration Diffusion Model

In this study, we aim to use a well-trained DDPM [13] to learn the prior distribution of images and ultimately solve non-blind and blind problems in various image restoration tasks.

### 2.1 Optimizable convolutional kernel as a universal degradation function

For a natural image  $x$ , its corresponding degraded image  $y$  can be obtained by the degradation function  $y = \mathcal{D}(x)$ . Most of the blind image restoration methods [10; 12] are used to solve the situation where the degradation function  $\mathcal{D}$  is known while leaving the parameters of  $\mathcal{D}$  are unknown. However, when dealing with real-world image restoration problems, the degradation function  $\mathcal{D}$  is not only an unknown quantity but also difficult to accurately represent mathematically. Therefore, we propose an optimized convolutional kernel to simulate complex degradation functions. The

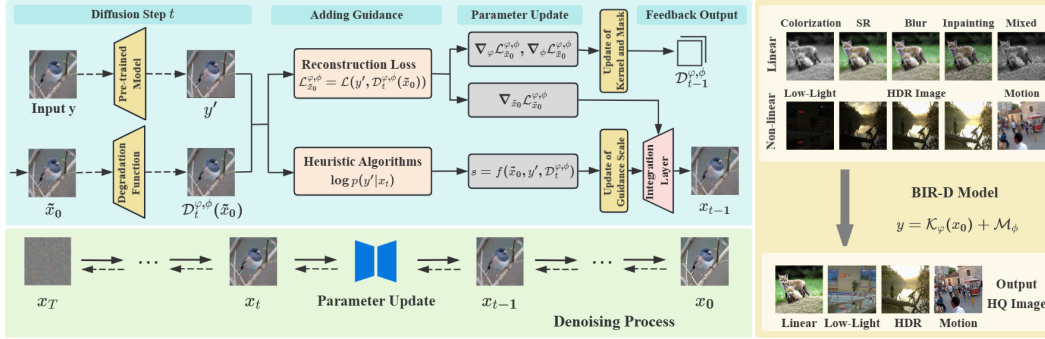


Figure 2: **Overview of BIR-D.** Degraded image  $y$  was given during the sampling process. BIR-D systematically incorporates guidance from degraded images in the reverse process of the diffusion model and optimizes the degraded model at the same time. For degraded image  $y$ , pre-training is first performed to provide a better initial state for BIR-D. BIR-D introduces a distance function in each step of the reverse process of the diffusion model to describe the distance loss between the degraded image  $y$  and the generated image  $\tilde{x}_0$  after the degradation function, so that the gradient could be used to update and simulate a better degradation function. Based on the empirical formula, the adaptive guidance scale can be calculated to provide optimal guidance during the sampling process.

parameters of the convolution kernel in the degradation function are dynamically optimized along with the denoising steps.

Moreover, in the real-world scenario, considering that there are different noises in different subtle areas of the image, using only one optimized convolutional kernel may not fully cover this situation. Therefore, we propose to utilize a mask  $\mathcal{M}$  to model and estimate these noises. Thus, the entire degradation process can be represented as:  $y = K(x) + \mathcal{M}$ , where  $\mathcal{K}$  refers to the optimized convolutional kernel used in the model and  $\mathcal{M}$  is a mask with the same dimension as image  $x$ .  $\mathcal{K}$  and  $\mathcal{M}$  have their own optimizable parameters, forming the degradation function *mathcalD*. In this way, any degradation process can be simulated by this degradation function.

## 2.2 Empirical formula of guidance scale

In the reverse denoising process of DDPM, the generated images can be conditioned on degraded image  $y$  [39]. Specifically, the distribution  $p_\theta(x_{t-1}|x_t)$  of reverse denoising is converted into

---

**Algorithm 1:** Unconditional diffusion model with the guidance of degraded image  $y$ , given a diffusion model noise prediction function  $\epsilon_\theta(x_t, t)$ .

---

**Input:** Degraded image  $y$ , degradation function  $\mathcal{D}$  composed of optimized convolutional kernels  $\mathcal{K}$  with parameters  $\varphi$  and mask  $\mathcal{M}$  with parameters  $\phi$ , learning rate  $l$ , distant measure  $\mathcal{L}$ .

**Output:** Output image  $x_0$  conditioned on  $y$ .

Sample  $x_T$  from  $\mathcal{N}(0, I)$

**for**  $t$  from  $T$  to  $1$  **do**

$$\begin{aligned} \tilde{x}_0 &= \frac{x_t}{\sqrt{\alpha_t}} - \frac{\sqrt{1-\alpha_t}\epsilon_\theta(x_t, t)}{\sqrt{\alpha_t}} \\ \mathcal{L}_{\varphi, \phi, \tilde{x}_0} &= \mathcal{L}(y, \mathcal{D}^{\varphi, \phi}(\tilde{x}_0)) \\ s &= -\frac{(x_t - \mu)^T g + C + \log N}{\mathcal{L}(\mathcal{D}^{\varphi, \phi}(\tilde{x}_0), y)} \\ \tilde{x}_0 &\leftarrow \tilde{x}_0 - \frac{s(1-\alpha_t)}{\sqrt{\alpha_{t-1}\beta_t}} \nabla_{\tilde{x}_0} \mathcal{L}_{\varphi, \phi, \tilde{x}_0} \\ \tilde{\mu}_t &= \frac{\sqrt{\alpha_{t-1}\beta_t}}{1-\alpha_t} \tilde{x}_0 + \frac{\sqrt{\alpha_t}(1-\alpha_{t-1})}{1-\alpha_t} x_t \\ \tilde{\beta}_t &= \frac{1-\alpha_{t-1}\beta_t}{1-\alpha_t} \beta_t \\ \text{Sample } x_{t-1} &\text{ from } \mathcal{N}(\tilde{\mu}_t, \tilde{\beta}_t I) \\ \varphi &\leftarrow \varphi - l \nabla_{\varphi} \mathcal{L}_{\varphi, \phi, \tilde{x}_0} \\ \phi &\leftarrow \phi - l \nabla_{\phi} \mathcal{L}_{\varphi, \phi, \tilde{x}_0} \end{aligned}$$

**return**  $x_0$

---



Figure 3: Comparison of image quality for blind face restoration results on LFW [14] and WIDER dataset [15].

Task	LFW dataset		WIDER dataset	
	FID	NIQE	FID	NIQE
PGDiff [16]	71.62	4.15	39.17	3.93
DiffBIR [17]	<b>39.58</b>	4.03	32.35	3.78
BIR-D	40.12	<b>3.94</b>	<b>31.49</b>	<b>3.65</b>

Table 1: Quantitative comparison of blind face restoration on LFW and WIDER datasets

a conditional distribution  $p_{\theta}(x_{t-1}|x_t, y)$ . It is demonstrated [13] that the difference between it and the original formula lies in the addition distribution of  $p(y|x_t)$ , which serves as a probability representation for denoising  $x_t$  into a high-quality image consistent with  $y$ . Previous work [10] proposed a feasible calculation to approximate this indicator by using heuristic algorithms:

$$\log p(y | x_t) = -\log N - s\mathcal{L}(\mathcal{D}(\tilde{x}_0), y), \quad (1)$$

where  $N$  is the normalization factor, which is the distribution  $p_{\theta}(y|x_{t+1})$ , and  $s$  is the scalar factor used to control the importance of guidance, named guidance scale.  $\mathcal{L}$  is the distance metric. The value of the guidance scale plays a crucial role in the quality of the image generation result. A larger value can lead to overall blurring of the image, while a smaller value can result in missing details in the restoration. However, the guidance scale in existing works [10; 9; 12] can only be manually set as a hyperparameter. But in specific experiments, the optimal value of the guidance scale varies in different masks, degraded images, and diffusion steps. The original configuration necessitates thorough testing for the initial setup. Additionally, employing the same guidance scale for every denoising step is not an optimal choice.

Therefore, we propose an empirical formula for the guidance scale, which can dynamically calculate and update the optimal values of guidance factors in real-time at each diffusion step of degraded images in specific repair tasks. Specifically, we noticed that the distribution  $\log p_{\theta}(y|x_t)$  can be applied to perform Taylor expansion around  $x = \mu$  and take the first two terms. The detailed process of proving can be found in Appendix D.

$$\log p_{\theta}(y | x_t) = (x_t - \mu)^T g + C, \quad (2)$$

where  $g = \nabla_{x_t} \log p_{\theta}(y | x_t) |_{x_t=\mu}$ ,  $C = \log p(y | x_t) |_{x_t=\mu}$ . By combining the heuristic approximation formula and Taylor expansion formula mentioned above, we can simplify the empirical

Task	4×Super resolution				Deblur				25% Inpainting				Colorization			
	PSNR	SSIM	Consistency	FID	PSNR	SSIM	Consistency	FID	PSNR	SSIM	Consistency	FID	PSNR	SSIM	Consistency	FID
RED[19]	24.18	0.71	27.57	98.30	21.30	0.58	63.20	69.55	-	-	-	-	-	-	-	-
DGP[18]	21.65	0.56	158.74	152.85	26.00	0.54	475.10	136.53	27.59	0.82	414.60	60.65	18.42	0.71	305.59	94.59
SNIPS[20]	22.38	0.66	21.38	154.43	24.73	0.69	60.11	17.11	17.55	0.74	587.90	103.50	-	-	-	-
DDRM[11]	<b>26.53</b>	0.78	19.39	40.75	<b>35.64</b>	<b>0.98</b>	50.24	4.78	34.28	0.95	<b>4.08</b>	24.09	<b>22.12</b>	0.91	37.33	47.05
DDNM[21]	25.36	<b>0.81</b>	7.52	39.14	24.66	0.71	41.70	4.64	32.16	<b>0.96</b>	5.42	17.63	21.95	0.89	36.41	38.79
GDP[10]	24.42	0.68	6.49	38.24	25.98	0.75	41.27	2.44	<b>34.40</b>	<b>0.96</b>	5.29	16.58	21.41	<b>0.92</b>	36.92	37.60
BIR-D	24.58	0.71	<b>6.32</b>	<b>37.54</b>	26.31	0.73	<b>38.42</b>	<b>2.32</b>	33.59	0.90	5.18	<b>15.73</b>	22.09	0.89	<b>36.12</b>	<b>36.58</b>

Table 2: Quantitative comparison of linear inverse problems on ImageNet 1k[18].

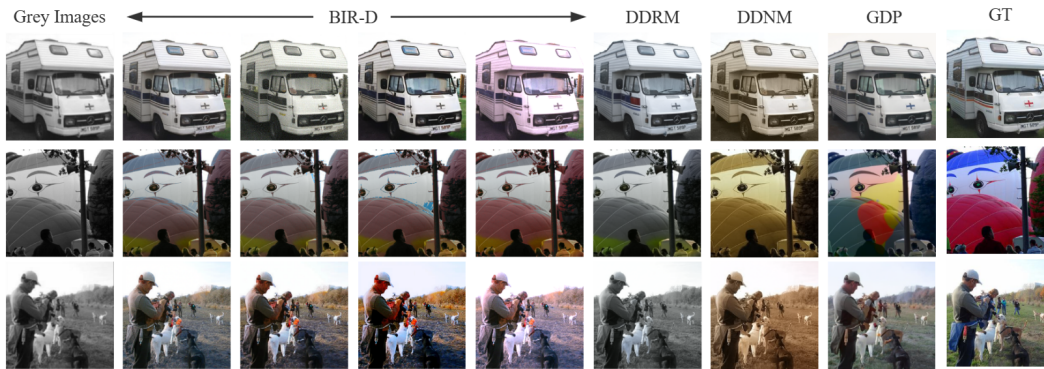


Figure 4: Comparison of colorization image on ImageNet 1k[18]. BIR-D can generate various outputs on the same input image.

formula for the guidance scale:

$$s = -\frac{(x_t - \mu)^T g + C + \log N}{\mathcal{L}(\mathcal{D}(\tilde{x}_0), y)}. \quad (3)$$

The guidance scale is related to the generated images  $x$ , degraded image  $y$ , and the degradation function  $\mathcal{D}$ . This value of this **Adaptive Guidance Scale** can be dynamically updated in each diffusion step so that each step in the diffusion model can use the most appropriate guidance scale.

### 2.3 Sampling process of BIR-D

Through empirical formulas, we can obtain the conditional transition formula in the reverse process of the diffusion model.

$$\log p_\theta(x_t|x_{t+1}, y) = \log(p_\theta(x_t|x_{t+1})p(y|x_t)) + N_1 \quad (4)$$

$$\approx \log p(z) + N_2, \quad (5)$$

where  $z$  conforms to the distribution  $\mathcal{N}(z; \mu_\theta(x_t, t) + \Sigma g, \Sigma)$ . The intermediate quantity  $g = \nabla_{x_t} \log p(y|x_t)$ . The value of  $g$  can be obtained by calculating the gradient in heuristic algorithms in eq. (1), which includes the parameter of guidance scale:

$$g = \nabla_{x_t} \log p(y|x_t) = -s \nabla_{x_t} \mathcal{L}(\mathcal{D}(x_t), y) \quad (6)$$

The other terms  $N_1$ ,  $N_2$ , and the variance of the reverse process  $\Sigma = \Sigma_\theta(x_t)$  in eq. (4) and eq. (5) are constants, and the unconditional distribution  $p_\theta(x_{t-1}|x_t)$  is given by traditional diffusion models.

Therefore, the conditional transition distribution  $p(x_{t-1}|x_t, y)$  can be approximately estimated by adding  $-(s \Sigma \nabla_{x_t} \mathcal{L}(\mathcal{D}(x_t), y))$  to the mean of the traditional unconditional transition distribution. Previous studies [10] have shown that the addition of  $\Sigma$  has a negative impact on the quality of generated images. Therefore, in this experiment, we omitted the term  $\Sigma$ , and the complete sampling process is shown in algorithm 1.

Detailly, in the diffusion step  $t$  of the sampling process, the noise of  $x_t$  is first predicted from the given pre-trained DDPM and eliminated to obtain an estimated value of  $x_0$ . Subsequently, apply the degradation function of step  $t$  to  $x_0$  and calculate its reconstruction loss with the degraded image

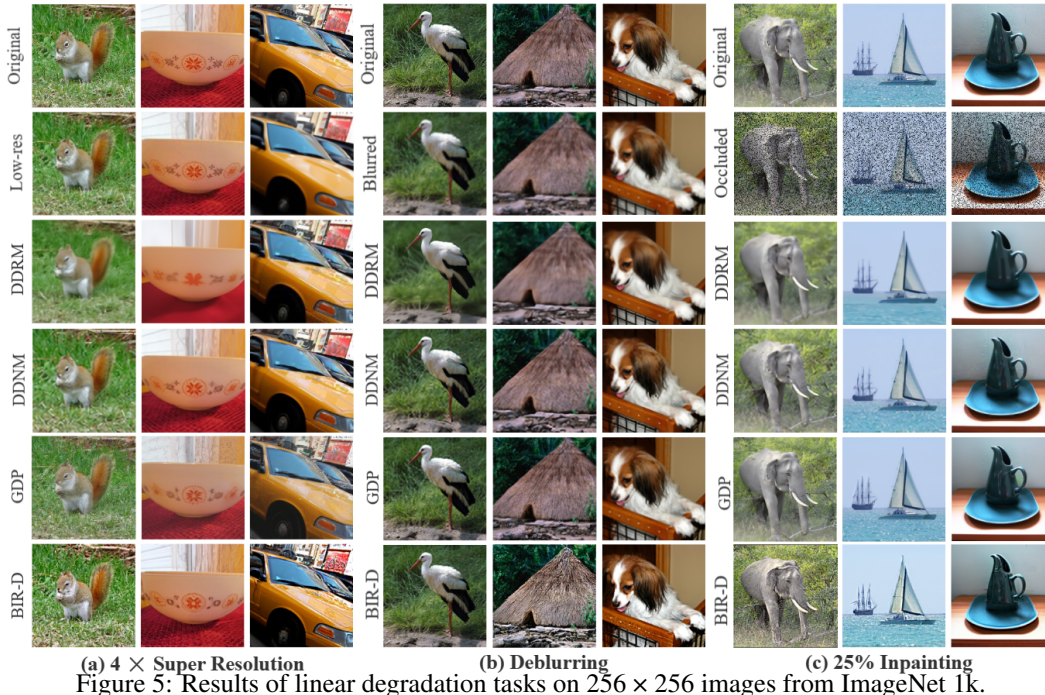


Figure 5: Results of linear degradation tasks on  $256 \times 256$  images from ImageNet 1k.

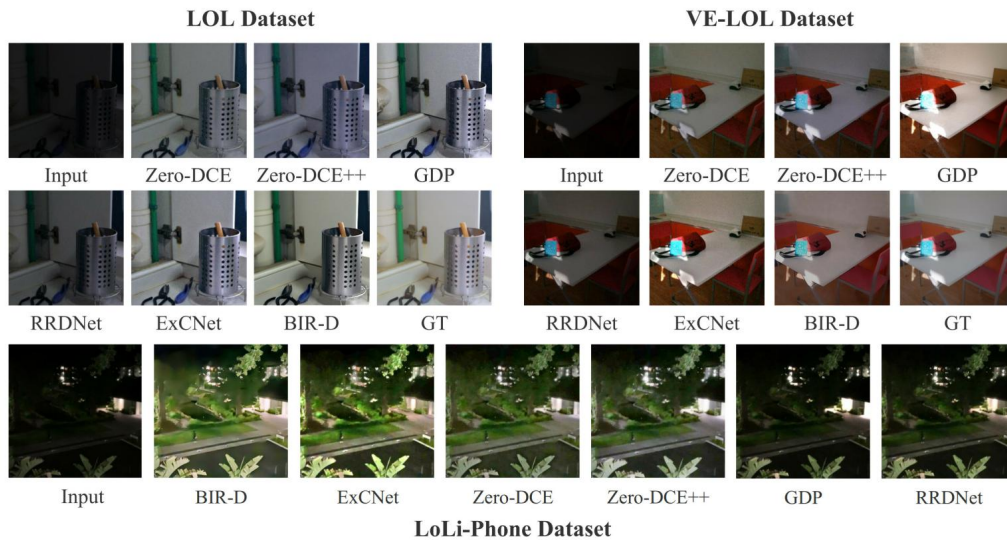


Figure 6: Comparison of image quality in low-light enhancement task on the LoL [22], VE-LoL [23] and LoLi-Phone [24] datasets.

*y*. We utilize our adaptive guidance scale for sampling the next step latent  $x_{t-1}$ . In this process, it is necessary to calculate the gradient about  $x_0$  and the parameters of each convolution kernel in the distance metric loss, which is used to update the convolution kernel parameters in real time for the next sampling process.

**Pre-process.** The empirical formula for the guidance scale we construct is related to the degradation function. Herein, when the model simulates the degradation function more reasonably, BIR-D can obtain more appropriate guidance scale values accordingly. To this end, we introduce a first-stage pre-training model from [17] to further enhance the model's capability to correct initial deviations. This enables the model to have a strong correction ability for significant deviations in the degradation function during the initial diffusion step, ultimately generating ideal image restoration results.

Task	LOL					VE-LOL-L				
	PSNR	SSIM	LOE	FID	PI	PSNR	SSIM	LOE	FID	PI
ExCNet[25]	<b>16.04</b>	0.62	220.38	111.18	8.70	16.20	0.66	225.15	115.24	8.62
Zero-DCE[26]	14.91	<b>0.70</b>	245.54	81.11	8.84	<b>17.84</b>	<b>0.73</b>	194.10	85.72	8.12
Zero-DCE++[27]	14.86	0.62	302.06	86.22	7.08	16.12	0.45	313.50	86.96	7.92
RRDNet[28]	11.37	0.53	127.22	89.09	8.17	13.99	0.58	94.23	83.41	7.36
GDP[10]	13.93	0.63	110.39	75.16	6.47	13.04	0.55	79.08	78.74	6.47
BIR-D	14.52	0.56	<b>105.42</b>	<b>68.98</b>	<b>4.87</b>	13.87	0.51	<b>78.18</b>	<b>74.54</b>	<b>5.73</b>

Table 3: Quantitative comparison among various zero-shot learning methods of low-light enhancement task on LOL [22] and VE-LOL-L [23] Bold font represents the best metric result.



Figure 7: Comparison of image quality for HDR image recovery results on NTIRE [29].

**Multi-degradation Image Restoration.** In the real world, the degradation process often involves a combination of multiple different complex types. To improve the image restoration capability of the model in complex situations and enhance its practicality, we propose to extend BIR-D into multi-task scenarios. To our surprise, BIR-D can fulfill multi-degradation image restoration without any modification (Figure 9) thanks to the mixture of degradation types can also be simulated as an unknown degradation by an optimizable convolutional kernel.

### 3 Experiments

In this section, we systematically compare BIR-D with other blind image restoration methods in real-world and synthetic datasets. We have attached some more specific details, such as the dataset, implementation, evaluation, and other results in the Appendix.

**Blind Image Restoration on Real-world Datasets.** Firstly, we evaluate the blind image restoration capability of BIR-D on two real-world datasets, namely LFW dataset [14] and WIDER dataset [15]. As shown in Figure 3, BIR-D successfully simulated and removed blur, and achieved more ideal facial detail restoration. The quantitative results in Table 1 shows that BIR-D outperforms PGDiff [16] and DiffBIR [17] in NIQE metric on both datasets and FID metric on WIDER, demonstrating better blind image restoration performance.

**Comparison on Common Linear Inverse Problems.** We conducted experiments on linear inverse problems on ImageNet 1k to compare BIR-D with off-the-shelf methods. For each experiment, we calculated the average Peak Signal-to-Noise Ratio (PSNR), Structural Similarity (SSIM), Consistency, and FID results, where PSNR, SSIM, and Consistency are used to quantify the faithfulness between the generated image and the original image, while FID is used to measure the quality of the generated image. To make fair comparisons, other methods are given known degradation functions as reported in the original paper while BIR-D utilizes universal degradation functions for different tasks. Table 2 shows that BIR-D outperforms other methods in terms of Consistency and FID in almost all tasks. As shown in Figure 5, the images generated by BIR-D demonstrate a high level of image quality and details. Moreover, Figure 4 also demonstrates that BIR-D can generate various results in image restoration tasks.

**Low Light Enhancement.** We further evaluated the effectiveness of BIR-D in low-light image enhancement. Following the previous works [10], we utilized three datasets, LOL [22], VE-LOL-L [23], and LoLi-Phone [24], to test the restoration ability of BIR-D. As shown in Table 3, our BIR-D outperforms all the zero-shot methods in both FID and Lightness Order Error (LOE) [40], and demonstrates significant improvement in Perceptual Index (PI) [41]. A lower PI value reflects better perceptual quality, while a lower LOE reflects a better natural preservation ability of the generated image, making images to have a more natural sensory experience. As shown in Figure 6 and the Appendix, BIR-D exhibits reasonable and well-exposed results.



Figure 8: Comparison of image quality for motion blur reduction results on GoPro [30] and HIDE dataset [31].

Motion Blur Reduction	GoPro		HIDE		HDR Recovery	NTIRE			
	PSNR	SSIM	PSNR	SSIM		PSNR	SSIM	LPIPS	FID
DeepRFT[32]	33.23	0.963	31.42	0.944	Deep-HDR[33]	21.66	0.76	0.26	57.52
MSDI-Net[34]	33.28	0.964	31.02	0.940	AHDRNet[35]	18.72	0.58	0.39	81.98
NAFNet[36]	33.69	0.967	31.32	0.943	HDR-GAN[37]	21.67	0.74	0.26	52.71
UFPNet[38]	34.06	<b>0.968</b>	31.74	0.947	GDP[10]	24.88	0.86	<b>0.13</b>	50.05
BIR-D	<b>34.12</b>	<b>0.968</b>	<b>32.09</b>	<b>0.948</b>	BIR-D	<b>25.03</b>	<b>0.88</b>	0.16	<b>48.74</b>

Table 4: Quantitative comparison of motion blur reduction and HDR image recovery tasks.

**HDR Image Recovery.** In the HDR image restoration task, we compared BIR-D with other leading methods, including DeepHDR [33], AHDRNet [35], HDR-GAN [37], and GDP [10], on the NTIRE2021 Multi-Frame HDR Challenge [29] dataset. The quantitative and qualitative results are presented in Table 4 and Figure 7, with BIR-D showing the best PSNR and SSIM levels, and successfully generating results with rich and accurate detailed information.

**Motion Blur Reduction.** To evaluate the performance of BIR-D in the motion blur reduction tasks, we compare BIR-D with the state-of-the-art motion blur reduction methods on GoPro dataset [30] and HIDE dataset [31]. We used the same input image, which also means that the motion blur of the input image is the same, ensuring fairness in comparison. The comparison results of the metrics are presented in Table 4, where BIR-D outperforms existing methods in both PSNR and SSIM. As shown in Figure 8, BIR-D can effectively achieve the elimination of motion blur. The generated images not only achieve a better quality but also receive restoration with more clear details.

**Multi-Degradation Image Restoration.** Encouraged by the excellent restoration performance of BIR-D on single restoration task, we further tested the image restoration performance of BIR-D in solving multi-task image restoration. As shown in Figure 9, we take a degraded image on the ImageNet

Methods	Dynamic Update		LOL					LoLi-Phone	
	Kernel	Guidance Scale	PSNR	SSIM	LOE	FID	PI	LOE	PI
Model A	✗	✗	8.96	0.46	210.88	113.36	8.24	110.05	8.36
Model B	✗	✓	9.58	0.48	203.83	102.47	7.90	102.55	8.25
Model C	✓	✗	14.35	0.54	113.56	82.14	5.23	75.34	7.94
BIR-D	✓	✓	<b>14.52</b>	<b>0.56</b>	<b>105.42</b>	<b>68.98</b>	<b>4.87</b>	<b>72.83</b>	<b>6.12</b>

Table 5: The ablation study on the optimizable convolutional kernel and the empirical settings of guidance scale.

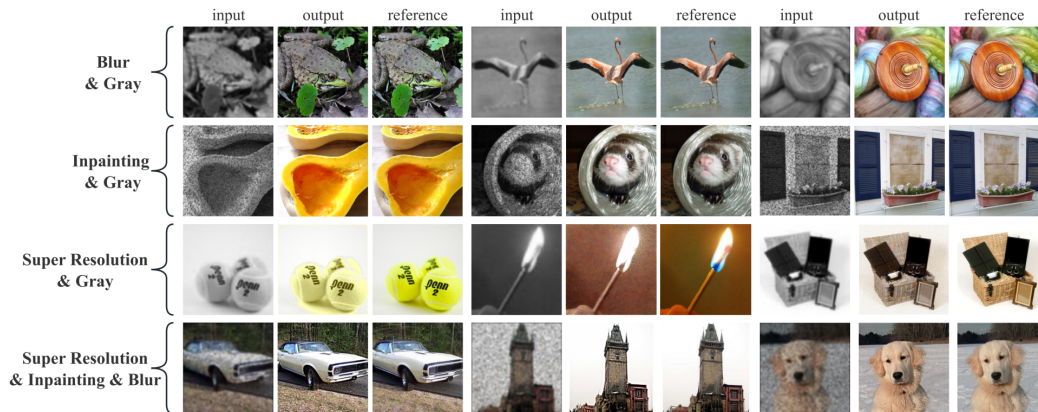


Figure 9: Results of multi-task image restoration.

Task	Random initial value				Biased initial value			
	PSNR	SSIM	Consistency	FID	PSNR	SSIM	Consistency	FID
BIR-D without pre-training model	25.88	0.69	40.24	2.55	21.49	0.61	53.78	4.32
BIR-D	26.31	0.73	38.42	2.32	25.97	0.71	39.87	2.41

Table 6: The ablation study on the effectiveness of the pre-training model.

dataset where two types of degradation are mixed as an example. The optimizable convolution kernel of BIR-D can also simulate these complicated degradation functions. The generated images obtained have excellent results in both image quality and details.

## 4 Ablation study

**The Effectiveness of Optimizable Convolutional Kernel and Adaptive Guidance Scale.** The ablation studies on the real-time optimizable convolutional kernel parameters and guidance scale were performed to reveal the effectiveness of these settings. We further tested the LOL [22] and the most challenging LoLi-phone [24] datasets. Model A fixed the convolutional kernel parameters and guidance scale. Models B and C represent fixed parameters for the convolution kernel and the fixed guidance scale, respectively. As illustrated in Figure 10, the fixed guidance scale with a bias set at  $s = 80000$  resulted in the emergence of mineral textures in the images. By contrast, as shown in Table 5, BIR-D outperformed other models in all indicators, demonstrating the effectiveness of an optimizable convolutional kernel and adaptive guidance scale.

**The Effectiveness of the First Stage Pre-training Model.** We conducted further experiments on the deblur task to demonstrate the impact of the first-stage pre-training model. As shown in Table 6, for a randomly initialized convolution kernel parameter, all metrics of BIR-D were better than BIR-D without the pre-training model. These results indicate that the first-stage pre-trained model is able to provide better initial state of images for our BIR-D.

## 5 Parameter analysis

**The Parameter Variations of the Optimizable Convolution Kernel and Mask in the Reverse Steps.** In order to visualize the variation trends of the parameters of convolution kernel mask in the reverse process, we conducted experiments on the test set of the LOL dataset from the low-light enhancement task. As shown in Figure 11(a), the mean values of the convolution kernel parameters and degradation mask are given by random initialization and gradually increase with the progress of the time steps. This increase in magnitude is influenced by the gradient of the distance metric with respect to the corresponding parameters. When the sampling step  $t < 500$ , the difference between  $\hat{x}_0$  and  $y$  changes slightly, resulting in correspondingly smaller gradient values.

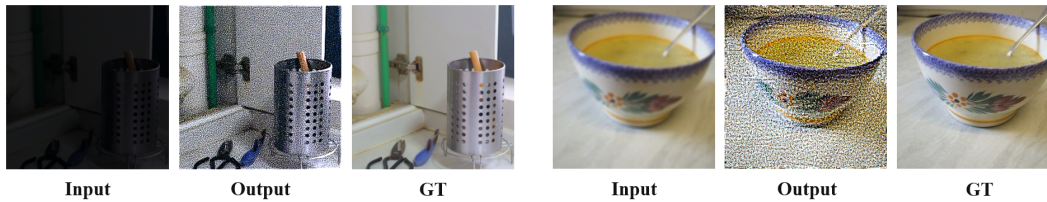


Figure 10: Qualitative results when the fixed guidance scale is biased towards a larger value of  $s = 80000$ .

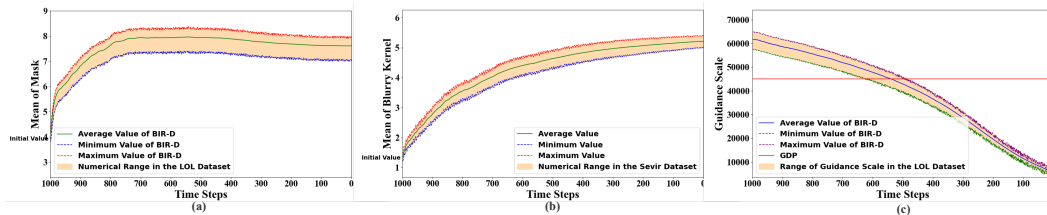


Figure 11: Illustration of (a) the variation of the mean of optimizable convolutional kernel parameters in each step of the sampling process. (b) The variation of the mean of degradation mask in each step of the sampling process. (c) The variation of adaptive guidance scale in each step of the sampling process. These experiments are performed on LOL dataset.

BIR-D employs masks in the degradation function with the intent to address the image restoration of local regions characterized by substantial shifts in brightness. Figure 11(b) shows that the mask  $\mathcal{M}$  of the degradation model has an upward trend from their initial values, making the overall degradation function approach the true degradation. As shown in Figure 12, during the sampling process, the degradation mask learns the detailed information of the image, including local regions with significant brightness differences. This process is obtained by updating the gradient of the distance metric with respect to the degradation mask parameters.

**The Theoretical Analysis of the Changing Trend of Guidance Scale in the Reverse Steps.** We take the variation in the guidance scale of BIR-D on the LOL dataset as an example to analyze the trend of its changes during the reverse steps. As shown in Figure 11(c), the guidance scale gradually decreases with the sampling step, which aligns with the actual situation. When the sampling step  $t < 500$ , as  $t$  decreases, the difference between  $x_t$  and  $x_{t-1}$  decreases with decreasing  $t$ , indicating a reduction in the simulated noise at each step. Therefore, the level of guidance required for each sampling step should also be reduced accordingly, leading to a decrease in the required guidance scale values. According to Equation (3), when step  $t$  is small, the gradient term  $g$  also decreases due to the small change in  $x_t$  at each step. The speed of the gradient term decreases is greater than the speed of distance metric decreases, resulting in a decrease in the value of the guidance scale.



Figure 12: The changing of degradation mask during the sampling process in HDR recovery.

## 6 Conclusion

In this paper, we propose Blind Image Restoration Diffusion, which is a unified model that can be used to solve various blind image restoration problems. We utilize optimized convolutional kernels to simulate and update the degradation function in the diffusion step in real time, and derive the empirical formula of the guidance scale in detail, so that it can better utilize the unconditional diffusion model to generate high-quality images. The ability to solve various blind image restoration tasks, including low-light enhancement and motion blur reduction, has also been verified through various indicators of datasets.

## Acknowledgment

The authors would like to thank Zhaoyang Lyu for his technical assistance. This work was supported by the National Natural Science Foundation of China (U2033209)

## References

- [1] Tao Yang, Peiran Ren, Xuansong Xie, and Lei Zhang. Gan prior embedded network for blind face restoration in the wild. In Proceedings of the IEEE/CVF conference on computer vision and pattern recognition, pages 672–681, 2021.
- [2] SG Gino Sophia, Syed Umar, and N Visvas. An efficient method for blind image restoration using gan. In 2022 international conference on innovative computing, intelligent communication and smart electrical systems (ICSSES), pages 1–8. IEEE, 2022.
- [3] Xu Deng, Hao Zhang, and Xiaojie Li. Hpg-gan: High-quality prior-guided blind face restoration generative adversarial network. Electronics, 12(16):3418, 2023.
- [4] Lin Luo, Jiaqi Bao, Jinlong Li, and Xiaorong Gao. Blind restoration of astronomical image based on deep attention generative adversarial neural network. Optical Engineering, 61(1):013101–013101, 2022.
- [5] Zhixin Wang, Ziyang Zhang, Xiaoyun Zhang, Huangjie Zheng, Mingyuan Zhou, Ya Zhang, and Yanfeng Wang. Dr2: Diffusion-based robust degradation remover for blind face restoration. In Proceedings of the IEEE/CVF Conference on Computer Vision and Pattern Recognition, pages 1704–1713, 2023.
- [6] Xunpeng Yi, Han Xu, Hao Zhang, Linfeng Tang, and Jiayi Ma. Diff-retinex: Rethinking low-light image enhancement with a generative diffusion model. In Proceedings of the IEEE/CVF International Conference on Computer Vision, pages 12302–12311, 2023.
- [7] Charles Laroche, Andrés Almansa, and Eva Coupete. Fast diffusion em: a diffusion model for blind inverse problems with application to deconvolution. In Proceedings of the IEEE/CVF Winter Conference on Applications of Computer Vision, pages 5271–5281, 2024.
- [8] Nan Wu, Guodong Wang, Hong Zhang, Guojia Hou, and Baoxiang Huang. Color blurred image restoration based on multichannel nonlinear diffusion model. In 2017 10th International Congress on Image and Signal Processing, BioMedical Engineering and Informatics (CISP-BMEI), pages 1–6. IEEE, 2017.
- [9] Yiman Zhu, Lu Wang, Jingyi Yuan, and Yu Guo. Diffusion model based low-light image enhancement for space satellite. arXiv preprint arXiv:2306.14227, 2023.
- [10] Ben Fei, Zhaoyang Lyu, Liang Pan, Junzhe Zhang, Weidong Yang, Tianyue Luo, Bo Zhang, and Bo Dai. Generative diffusion prior for unified image restoration and enhancement. In Proceedings of the IEEE/CVF Conference on Computer Vision and Pattern Recognition, pages 9935–9946, 2023.
- [11] Bahjat Kawar, Michael Elad, Stefano Ermon, and Jiaming Song. Denoising diffusion restoration models. Advances in Neural Information Processing Systems, 35:23593–23606, 2022.
- [12] Yinhuai Wang, Jiwen Yu, Runyi Yu, and Jian Zhang. Unlimited-size diffusion restoration. In Proceedings of the IEEE/CVF Conference on Computer Vision and Pattern Recognition, pages 1160–1167, 2023.
- [13] Prafulla Dhariwal and Alexander Nichol. Diffusion models beat gans on image synthesis. Advances in neural information processing systems, 34:8780–8794, 2021.
- [14] Xintao Wang, Yu Li, Honglun Zhang, and Ying Shan. Towards real-world blind face restoration with generative facial prior. In Proceedings of the IEEE/CVF conference on computer vision and pattern recognition, pages 9168–9178, 2021.

- [15] Shangchen Zhou, Kelvin Chan, Chongyi Li, and Chen Change Loy. Towards robust blind face restoration with codebook lookup transformer. Advances in Neural Information Processing Systems, 35:30599–30611, 2022.
- [16] Peiqing Yang, Shangchen Zhou, Qingyi Tao, and Chen Change Loy. Pgdiffr: Guiding diffusion models for versatile face restoration via partial guidance. Advances in Neural Information Processing Systems, 36, 2024.
- [17] Xinqi Lin, Jingwen He, Ziyang Chen, Zhaoyang Lyu, Ben Fei, Bo Dai, Wanli Ouyang, Yu Qiao, and Chao Dong. Diffbir: Towards blind image restoration with generative diffusion prior. arXiv preprint arXiv:2308.15070, 2023.
- [18] Xingang Pan, Xiaohang Zhan, Bo Dai, Dahua Lin, Chen Change Loy, and Ping Luo. Exploiting deep generative prior for versatile image restoration and manipulation. IEEE Transactions on Pattern Analysis and Machine Intelligence, 44(11):7474–7489, 2021.
- [19] Yaniv Romano, Michael Elad, and Peyman Milanfar. The little engine that could: Regularization by denoising (red). SIAM Journal on Imaging Sciences, 10(4):1804–1844, 2017.
- [20] Bahjat Kawar, Gregory Vaksman, and Michael Elad. Snips: Solving noisy inverse problems stochastically. Advances in Neural Information Processing Systems, 34:21757–21769, 2021.
- [21] Yinhuai Wang, Jiwen Yu, and Jian Zhang. Zero-shot image restoration using denoising diffusion null-space model. arXiv preprint arXiv:2212.00490, 2022.
- [22] C Wei, W Wang, W Yang, and J Liu. Deep retinex decomposition for low-light enhancement. arxiv 2018. arXiv preprint arXiv:1808.04560, 1808.
- [23] Jiaying Liu, Dejia Xu, Wenhan Yang, Minhao Fan, and Haofeng Huang. Benchmarking low-light image enhancement and beyond. International Journal of Computer Vision, 129:1153–1184, 2021.
- [24] Chongyi Li, Chunle Guo, Linghao Han, Jun Jiang, Ming-Ming Cheng, Jinwei Gu, and Chen Change Loy. Low-light image and video enhancement using deep learning: A survey. IEEE Transactions on Pattern Analysis and Machine Intelligence, 44(12):9396–9416, 2021.
- [25] Lin Zhang, Lijun Zhang, Xiao Liu, Ying Shen, Shaoming Zhang, and Shengjie Zhao. Zero-shot restoration of back-lit images using deep internal learning. In Proceedings of the 27th ACM International Conference on Multimedia, pages 1623–1631, 2019.
- [26] Chunle Guo, Chongyi Li, Jichang Guo, Chen Change Loy, Junhui Hou, Sam Kwong, and Runmin Cong. Zero-reference deep curve estimation for low-light image enhancement. In Proceedings of the IEEE/CVF Conference on Computer Vision and Pattern Recognition, pages 1780–1789, 2020.
- [27] Chongyi Li, Chunle Guo, and Chen Change Loy. Learning to enhance low-light image via zero-reference deep curve estimation. IEEE Transactions on Pattern Analysis and Machine Intelligence, 44(8):4225–4238, 2021.
- [28] Anqi Zhu, Lin Zhang, Ying Shen, Yong Ma, Shengjie Zhao, and Yicong Zhou. Zero-shot restoration of underexposed images via robust retinex decomposition. In 2020 IEEE International Conference on Multimedia and Expo (ICME), pages 1–6. IEEE, 2020.
- [29] Eduardo Pérez-Pellitero, Sibi Catley-Chandar, Ales Leonardis, and Radu Timofte. Ntire 2021 challenge on high dynamic range imaging: Dataset, methods and results. In Proceedings of the IEEE/CVF Conference on Computer Vision and Pattern Recognition, pages 691–700, 2021.
- [30] Seungjun Nah, Tae Hyun Kim, and Kyoung Mu Lee. Deep multi-scale convolutional neural network for dynamic scene deblurring. In Proceedings of the IEEE conference on computer vision and pattern recognition, pages 3883–3891, 2017.
- [31] Ziyi Shen, Wenguan Wang, Xiankai Lu, Jianbing Shen, Haibin Ling, Tingfa Xu, and Ling Shao. Human-aware motion deblurring. In Proceedings of the IEEE/CVF International Conference on Computer Vision, pages 5572–5581, 2019.

- [32] Xintian Mao, Yiming Liu, Fengze Liu, Qingli Li, Wei Shen, and Yan Wang. Intriguing findings of frequency selection for image deblurring. In Proceedings of the AAAI Conference on Artificial Intelligence, volume 37, pages 1905–1913, 2023.
- [33] Shangzhe Wu, Jiarui Xu, Yu-Wing Tai, and Chi-Keung Tang. Deep high dynamic range imaging with large foreground motions. In Proceedings of the European Conference on Computer Vision (ECCV), pages 117–132, 2018.
- [34] Dasong Li, Yi Zhang, Ka Chun Cheung, Xiaogang Wang, Hongwei Qin, and Hongsheng Li. Learning degradation representations for image deblurring. In European Conference on Computer Vision, pages 736–753. Springer, 2022.
- [35] Qingsen Yan, Dong Gong, Qinfeng Shi, Anton van den Hengel, Chunhua Shen, Ian Reid, and Yanning Zhang. Attention-guided network for ghost-free high dynamic range imaging. In Proceedings of the IEEE/CVF Conference on Computer Vision and Pattern Recognition, pages 1751–1760, 2019.
- [36] Liangyu Chen, Xiaojie Chu, Xiangyu Zhang, and Jian Sun. Simple baselines for image restoration. In European conference on computer vision, pages 17–33. Springer, 2022.
- [37] Yuzhen Niu, Jianbin Wu, Wenxi Liu, Wenzhong Guo, and Rynson WH Lau. Hdr-gan: Hdr image reconstruction from multi-exposed ldr images with large motions. IEEE Transactions on Image Processing, 30:3885–3896, 2021.
- [38] Zhenxuan Fang, Fangfang Wu, Weisheng Dong, Xin Li, Jinjian Wu, and Guangming Shi. Self-supervised non-uniform kernel estimation with flow-based motion prior for blind image deblurring. In Proceedings of the IEEE/CVF conference on computer vision and pattern recognition, pages 18105–18114, 2023.
- [39] Georgios Batzolis, Jan Stanczuk, Carola-Bibiane Schönlieb, and Christian Etmann. Conditional image generation with score-based diffusion models. arXiv preprint arXiv:2111.13606, 2021.
- [40] Shuhang Wang, Jin Zheng, Hai-Miao Hu, and Bo Li. Naturalness preserved enhancement algorithm for non-uniform illumination images. IEEE transactions on image processing, 22(9):3538–3548, 2013.
- [41] Anish Mittal, Rajiv Soundararajan, and Alan C Bovik. Making a “completely blind” image quality analyzer. IEEE Signal processing letters, 20(3):209–212, 2012.
- [42] Jonathan Ho, Ajay Jain, and Pieter Abbeel. Denoising diffusion probabilistic models. Advances in neural information processing systems, 33:6840–6851, 2020.
- [43] Alexander Quinn Nichol and Prafulla Dhariwal. Improved denoising diffusion probabilistic models. In International conference on machine learning, pages 8162–8171. PMLR, 2021.
- [44] Bahjat Kawar, Jiaming Song, Stefano Ermon, and Michael Elad. Jpeg artifact correction using denoising diffusion restoration models. In Neural Information Processing Systems (NeurIPS) Workshop on Score-Based Methods, 2022.
- [45] Ozan Özdenizci and Robert Legenstein. Restoring vision in adverse weather conditions with patch-based denoising diffusion models. IEEE Transactions on Pattern Analysis and Machine Intelligence, 2023.
- [46] Ziwei Luo, Fredrik K Gustafsson, Zheng Zhao, Jens Sjölund, and Thomas B Schön. Refusion: Enabling large-size realistic image restoration with latent-space diffusion models. In Proceedings of the IEEE/CVF conference on computer vision and pattern recognition, pages 1680–1691, 2023.
- [47] Ruxin Wang and Dacheng Tao. Training very deep cnns for general non-blind deconvolution. IEEE Transactions on Image Processing, 27(6):2897–2910, 2018.
- [48] Ben Fei, Yixuan Li, Weidong Yang, Hengjun Gao, Jingyi Xu, Lipeng Ma, Yatian Yang, and Pinghong Zhou. Lightening anything in medical images. arXiv preprint arXiv:2406.10236, 2024.

- [49] M Anand, A Ashwin Natraj, V Jeya Maria Jose, K Subramanian, Priyanka Bhardwaj, R Pandeeswari, and S Deivalakshmi. Tackling multiple visual artifacts: Blind image restoration using conditional adversarial networks. In Computer Vision and Image Processing: 4th International Conference, CVIP 2019, Jaipur, India, September 27–29, 2019, Revised Selected Papers, Part II 4, pages 331–342. Springer, 2020.
- [50] Raymond A Yeh, Teck Yian Lim, Chen Chen, Alexander G Schwing, Mark Hasegawa-Johnson, and Minh N Do. Image restoration with deep generative models. In 2018 IEEE International Conference on Acoustics, Speech and Signal Processing (ICASSP), pages 6772–6776. IEEE, 2018.
- [51] Fangzhou Luo and Xiaolin Wu. Maximum a posteriori on a submanifold: a general image restoration method with gan. In 2020 International Joint Conference on Neural Networks (IJCNN), pages 1–7. IEEE, 2020.
- [52] Fangzhou Luo, Xiaolin Wu, and Yanhui Guo. And: Adversarial neural degradation for learning blind image super-resolution. Advances in Neural Information Processing Systems, 36, 2024.
- [53] Hyungjin Chung, Jeongsol Kim, Sehui Kim, and Jong Chul Ye. Parallel diffusion models of operator and image for blind inverse problems. In Proceedings of the IEEE/CVF Conference on Computer Vision and Pattern Recognition, pages 6059–6069, 2023.
- [54] Vaishnav Potlapalli, Syed Waqas Zamir, Salman Khan, and Fahad Shahbaz Khan. Promptir: Prompting for all-in-one blind image restoration. arXiv preprint arXiv:2306.13090, 2023.

In this appendix, we provide a more detailed derivation process for adaptive guidance scale and more image restoration results. Appendix A provides more blind image restoration results for images undergoing various multi-degradation modes. Appendix B is a preliminary for the diffusion model. Appendix C introduces the related work, including an introduction to diffusion-based image restoration models and existing leading methods in the field of blind image restoration. Appendix D is the complete derivation process of the empirical setting of the adaptive guidance scale. Appendix E proposes the algorithmic process of BIR-D for accomplishing multi-guidance blind image restoration. Appendix F conducts further ablation experiments on the size and other parameters of the convolution kernel and provides the optimal convolution kernel parameter settings for different image restoration tasks. Appendix G presents and analyzes the variations of the mask parameters in the reverse steps of LOL dataset. Appendix H presents the results of blind image restoration tasks, including blind face restoration, low-light enhancement, motion blur reduction, and HDR image restoration. Appendix I provides more results on the ImageNet dataset for four basic tasks, including super-resolution, colorization, deblurring and inpainting, as well as corresponding experimental details and parameter settings. Appendix J discusses limitations and future works for BIR-D.

## A Multi-degradation Image Restoration

In this section, we attempted more complex degradation scenarios to test the image restoration ability of BIR-D. The input images are derived from adding different degradation types, which include  $4 \times$  super-resolution, colorization, deblurring, and inpainting. As shown in Figure 13, BIR-D achieved satisfactory restoration results in four different multi-task image restoration tasks, which indicates the image restoration capability of BIR-D under complex degraded scenarios.

## B Preliminary

Diffusion models consists of the forward and reverse processes. The forward process continuously adds noise to a natural image  $x_0$  through  $T$  diffusion steps to obtain the noise distribution  $x_T \sim \mathcal{N}(0, I)$ , where  $\mathcal{N}$  represents the Gaussian distribution. The reverse process aims to simulate the noise in each diffusion step and eliminate it, ultimately obtaining the restored generated image  $x_0$ .

The forward process is a Markov chain defined by the following equation:

$$q(x_1, \dots, x_T | x_0) = \prod_{t=1}^T q(x_t | x_{t-1}) \quad (7)$$

It corrupts the initial data  $x_0$  into distribution  $x_T$  that is close to Gaussian noise after  $T$  steps of diffusion, with each sample process defined by  $q(x_t | x_{t-1}) = \mathcal{N}(x_t; \sqrt{1 - \beta_t}x_{t-1}, \beta_t I)$ , where  $\beta_t$  is the variance of a forward process. The variance can be set as a constant or learned by reparameterization. Simultaneously defining  $\alpha_t = 1 - \beta_t, \bar{\alpha}_t = \prod_{i=1}^t \alpha_i$ . It has been proven by [42] that through mathematical reasoning,  $x_t$  at any diffusion step can be directly calculated from the starting  $x_0$ :

$$x_t = \sqrt{\bar{\alpha}_t}x_0 + \sqrt{1 - \bar{\alpha}_t}\epsilon, \quad (8)$$

where  $\epsilon \sim \mathcal{N}(0, I)$ . When  $T$  is large enough,  $\sqrt{\bar{\alpha}_t}$  approaches 0, and at this point  $q(x_T | x_0)$  is closer to the latent distribution of  $x_T$ .

The reverse process is also a Markov chain, which gradually denoises a standard multivariate Gaussian distribution into a denoised image  $x_0$ . Firstly, sample  $x_t \sim \mathcal{N}(0, I)$ . The conditional distribution of the reverse process is  $p_\theta(x_{t-1} | x_t) = \mathcal{N}(x_{t-1}; \mu_\theta(x_t, t), \Sigma_\theta I)$ . According to the Bayesian formula, it can be transformed as follows:

$$q(x_{t-1} | x_t, x_0) = q(x_t | x_{t-1}, x_0) \frac{q(x_{t-1} | x_0)}{q(x_t | x_0)} \quad (9)$$

Expand and simplify the three terms at the right end of the equation. The variance  $\Sigma_\theta$  of the reverse process can be obtained as a fixed value. Note that [43] indicates that it can also be learned parameters. And the mean of the reverse process  $\mu_\theta$  related to  $x_t$  and  $\tilde{x}_0$ :

$$\tilde{\mu}_t(x_t, \tilde{x}_0) = \frac{\sqrt{\bar{\alpha}_t - 1}\beta_t}{1 - \bar{\alpha}_t} \tilde{x}_0 + \frac{\bar{\alpha}_t(1 - \bar{\alpha}_{t-1})}{1 - \bar{\alpha}_t} x_t \quad (10)$$

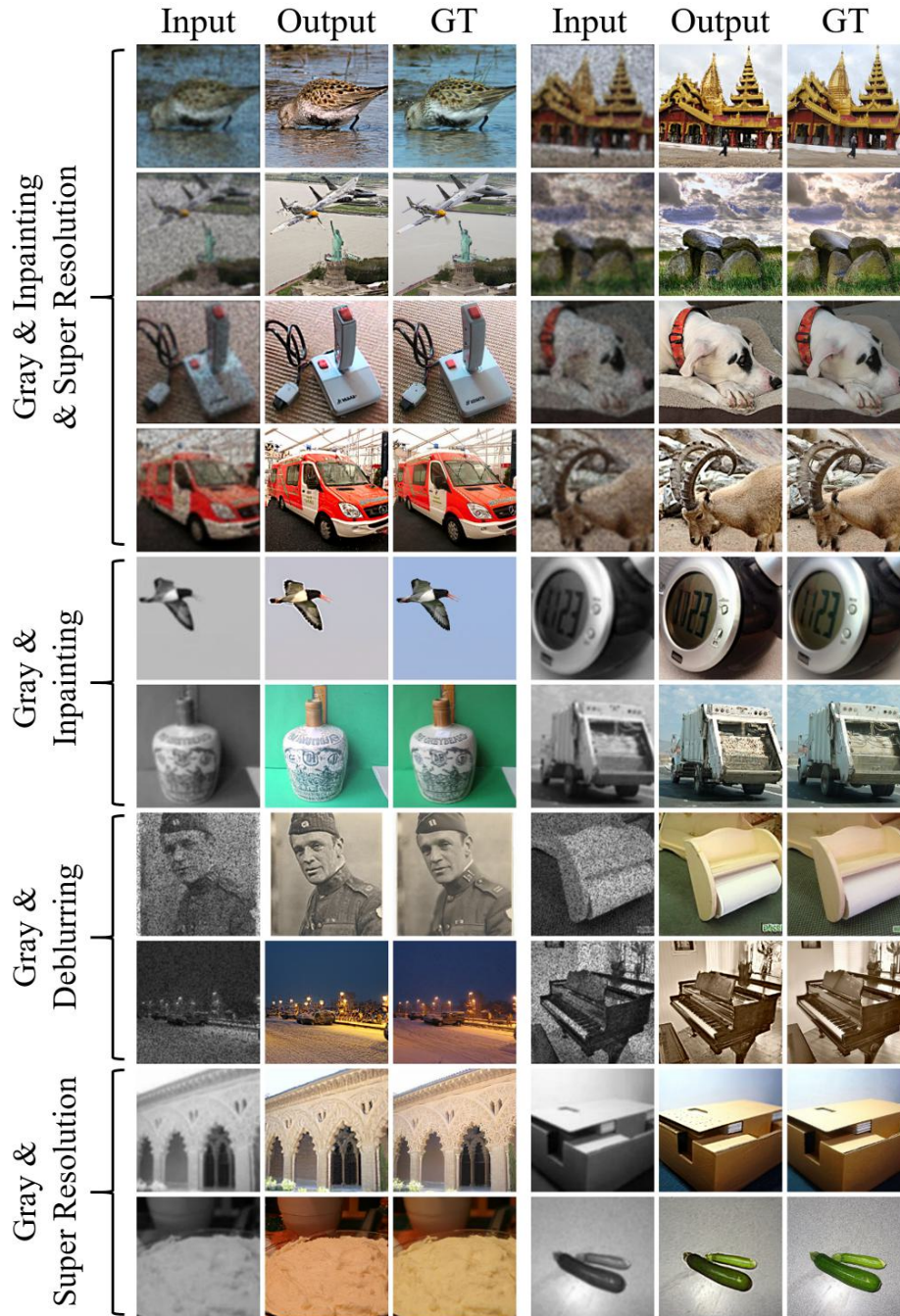


Figure 13: Image results of BIR-D in multi-degradation tasks on the ImageNet dataset. Each row in the figure consists of two sets of images, and the left, middle and right images of each set represent input, output, and ground truth respectively.

According to the formula of the forward process,  $\tilde{x}_0$  can be predicted by  $x_t$ , where  $\epsilon$  is a noise function approximator obtained by a neural network  $\theta$ .

$$\tilde{x}_0 = \frac{x_t}{\sqrt{\alpha_t}} - \frac{\sqrt{1 - \alpha_t} \epsilon_\theta(x_t, t)}{\sqrt{\alpha_t}} \quad (11)$$

Substitute it into Equation (10) to obtain the mean value  $\mu_\theta$ :

$$\mu_\theta(x_t, t) = \frac{1}{\sqrt{\alpha_t}} \left( x_t - \frac{\beta_t}{\sqrt{1 - \alpha_t}} \epsilon_\theta(x_t, t) \right) \quad (12)$$

## C Related Work

**Diffusion Model for Image Restoration.** Image restoration and denoising have seen various advancements with diffusion-based models [16; 17]. They have been thoroughly explored for linear inverse problems [11; 10], nonlinear inverse problems [44; 10]. To alleviate the fixed- and small-size generation of diffusion models, patch-based algorithm [45] and large-size generation [46; 12] are proposed. Our model introduces the guidance of degraded images to form an unconditional diffusion model, and attempts to simulate and update the degradation function in real-time, making it suitable for general tasks while maintaining both image quality and efficiency.

**Blind Image Restoration.** Many problem-solving approaches have emerged in the field of blind image restoration [47; 48]. The emergence of GANs [2; 49] provides several solutions for unsupervised learning in blind image restoration. Generative prior-based image restoration methods [50; 51] employ deep generative models to learn the prior and demonstrate that GAN can be employed as a density estimation model to address various image restoration task. Besides, [51; 52] can also generate a broad spectrum of highly nonlinear complex degradation without any explicit supervision through training in concert with a deep restoration neural network governed by a minmax criterion. On top of GANs and other relevant methods, DDPMs are more studied for this task due to the enhanced diversity. For instance, both DiffBIR [17] and GDP [10] leverage generative diffusion priors for blind image restoration. BlindDPS [53] introduces parallel diffusion models for solving blind inverse problems when the functional forms are known. PromptIR [54] uses prompts to encode degradation-specific information and dynamically guide the recovery of the network. Nevertheless, these methods are still limited to specific tasks. BIR-D can be regarded as a unified solver for multiple restoration tasks by simultaneously estimating the recovered images and specific degradation models.

## D Adaptive Guidance Scale

In the reverse process of the diffusion model, we added guidance from  $y$  to transform the original reverse denoising distribution  $p_\theta(x_t | x_{t+1})$  into a conditional distribution  $p_\theta(x_t | x_{t+1}, y)$ . This distribution can be further simplified:

$$p_\theta(x_t | x_{t+1}, y) = \frac{p_\theta(x_t, x_{t+1}, y)}{p_\theta(x_{t+1}, y)} \quad (13)$$

$$= \frac{p_\theta(x_t, x_{t+1}, y)}{p_\theta(y | x_{t+1}) p_\theta(x_{t+1})} \quad (14)$$

$$= \frac{p_\theta(x_t | x_{t+1}) p_\theta(y | x_t, x_{t+1}) p_\theta(x_{t+1})}{p_\theta(y | x_{t+1}) p_\theta(x_{t+1})} \quad (15)$$

$$= \frac{p_\theta(y | x_t, x_{t+1}) p_\theta(x_t | x_{t+1})}{p_\theta(y | x_{t+1})} \quad (16)$$

$$= \frac{p_\theta(y | x_t) p_\theta(x_t | x_{t+1})}{p_\theta(y | x_{t+1})} \quad (17)$$

$$= \frac{p(y | x_t) p_\theta(x_t | x_{t+1})}{p_\theta(y | x_{t+1})} \quad (18)$$

In this formula, distribution  $p_\theta(y | x_{t+1})$  is independent of  $x_t$ , so we use the constant  $N$  instead:

$$p_\theta(x_t | x_{t+1}, y) = \frac{1}{N} p_\theta(x_t | x_{t+1}) p_\theta(y | x_t) \quad (19)$$

Therefore, compared to the original diffusion model, the conditional reverse process requires approximation of  $p_\theta(y | x_t)$ . We used a heuristic approximation method:

$$p(y | x_t) = \frac{1}{N} \exp(-s\mathcal{L}(\mathcal{D}(x_t), y)) \quad (20)$$

Where  $\mathcal{L}$  is image distance metric, which represents the MSE loss in this experiment.  $K$  is the constant in the above formula, which serves as a normalization factor here. And  $s$  is a guidance scale, which is used to control the magnitude of guidance. Take the logarithm of both sides of the equation:

$$\log p(y | x_t) = -\log N - s\mathcal{L}(\mathcal{D}(x_t), y) \quad (21)$$

When the diffusion step approaches infinity,  $\|\Sigma\| \rightarrow 0$ , so we can assume that distribution  $\log p_\theta(y | x_t)$  has low curvature compared to  $\Sigma^{-1}$ . We can perform Taylor expansion on distribution  $\log p_\theta(y | x_t)$  around  $x = \mu$  and take the first two terms:

$$\log p_\theta(y | x_t) \approx \log p(y | x_t) |_{x_t=\mu} + (x_t - \mu)^T \nabla_{x_t} \log p_\theta(y | x_t) |_{x_t=\mu} \quad (22)$$

$$= (x_t - \mu)^T g + C \quad (23)$$

Where  $g = \nabla_{x_t} \log p_\theta(y | x_t) |_{x_t=\mu}$ ,  $C = \log p(y | x_t) |_{x_t=\mu}$ . By combining the heuristic approximation formula and Taylor expansion formula mentioned above, we can simplify the empirical formula for the guidance scale:

$$-\log N - s\mathcal{L}(\mathcal{D}(x_t), y) = (x_t - \mu)^T g + C \quad (24)$$

The empirical formula is shown below. For each image at every moment  $t$ , the applicable value of the guidance scale can be calculated.

$$s = -\frac{(x_t - \mu)^T g + C + \log N}{\mathcal{L}(\mathcal{D}(x_t), y)} \quad (25)$$

Because here  $y$  is a loss image without noise, while  $x_t$  itself has noise. The use of MSE errors between  $x_t$  and  $y$  can lead to the introduction of noise into the guidance process. Therefore, we are using the MSE error between the estimated value of  $\tilde{x}_0$  and  $y$  here, and the above formula needs to be corrected as:

$$s = -\frac{(x_t - \mu)^T g + C + \log N}{\mathcal{L}(\mathcal{D}(\tilde{x}_0), y)} \quad (26)$$

## E Multi-Guidance Blind Image Restoration

BIR-D is capable of accepting multiple input images to incorporate multi-guidance during the reverse steps. Taking HDR image restoration task as an example, BIR-D receives three images as inputs separately. As shown in Figure 14 and Algorithm 2, BIR-D uses three degradation functions for three input images. In each sampling step, after obtaining  $\tilde{x}_0$ ,  $\tilde{x}_0$  is respectively substituted into three degradation function at diffusion step  $t$ . The parameters of convolution kernels and masks are updated by measuring the gradient of its parameters with the distance metric. The average of three distance metrics are used as the overall loss to update the mean and variance used during sampling. The empirical formula of adaptive guidance scale is also based on this loss.

## F The Optimal Size of Optimizable Convolutional Kernel.

In the main paper, in order to assure the versatility of BIR-D, we used convolution kernels of size  $7 \times 7$  for all tasks. Nevertheless, for different types of tasks, the size of the convolution kernel might

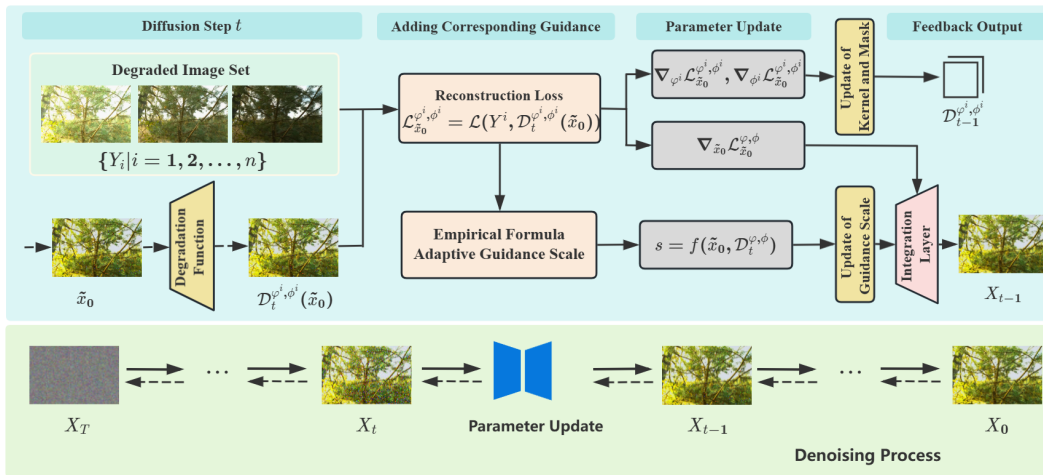


Figure 14: BIR-D image restoration pipeline for multi-guidance tasks.

**Algorithm 2:** BIR-D with the multi-guidance of degraded images set  $\{y^i | i = 1, 2, \dots, n\}$  (For HDR image restoration tasks,  $n=3$ ), given a diffusion model noise prediction function  $\epsilon_\theta(x_t, t)$ .

**Input:** Degraded image set  $\{y^i | i = 1, 2, \dots, n\}$ . For each image  $y^i$  in the set, there is a corresponding degradation function  $\mathcal{D}^i$  composed of optimized convolutional kernels  $\mathcal{K}^i$  with parameters  $\varphi^i$  and mask  $\mathcal{M}^i$  with parameters  $\phi^i$ , learning rate  $l$ , distant measure  $\mathcal{L}^i$ .

**Output:** Output image  $x_0$  conditioned on set  $\{y^i | i = 1, 2, \dots, n\}$ .

Sample  $x_T$  from  $\mathcal{N}(0, I)$

**for**  $t$  from  $T$  to  $1$  **do**

$$\tilde{x}_0 = \frac{x_t}{\sqrt{\alpha_t}} - \frac{\sqrt{1-\alpha_t}\epsilon_\theta(x_t, t)}{\sqrt{\alpha_t}}$$

**for**  $i$  from  $1$  to  $n$  **do**

$$\mathcal{L}_{\varphi^i, \phi^i, \tilde{x}_0} = \mathcal{L}(y^i, \mathcal{D}^{\varphi^i, \phi^i}(\tilde{x}_0))$$

$$\varphi^i \leftarrow \varphi^i - l \nabla_{\varphi^i} \mathcal{L}_{\varphi^i, \phi^i, \tilde{x}_0}$$

$$\phi^i \leftarrow \phi^i - l \nabla_{\phi^i} \mathcal{L}_{\varphi^i, \phi^i, \tilde{x}_0}$$

$$\mathcal{L}_{\varphi, \phi, \tilde{x}_0} = \sum_{i=1}^n \mathcal{L}_{\varphi^i, \phi^i, \tilde{x}_0}$$

$$s = -\frac{(x_t - \mu)^T g + C + \log N}{\mathcal{L}_{\varphi, \phi, \tilde{x}_0}}$$

$$\tilde{x}_0 \leftarrow \tilde{x}_0 - \frac{s(1-\alpha_t)}{\sqrt{\alpha_t-1}\beta_t} \nabla_{\tilde{x}_0} \mathcal{L}_{\varphi, \phi, \tilde{x}_0}$$

$$\tilde{\mu}_t = \frac{\sqrt{\alpha_t-1}\beta_t}{1-\alpha_t} \tilde{x}_0 + \frac{\sqrt{\alpha_t}(1-\alpha_t-1)}{1-\alpha_t} x_t$$

$$\tilde{\beta}_t = \frac{1-\alpha_t-1}{1-\alpha_t} \beta_t$$

Sample  $x_{t-1}$  from  $\mathcal{N}(\tilde{\mu}_t, \tilde{\beta}_t I)$

**return**  $x_0$

Task	Low-Light Enhancement					Motion Blur Reduction	
	PSNR	SSIM	LOE	FID	PI	PSNR	SSIM
kernel size=1	13.73	0.49	118.38	78.52	5.67	31.14	0.917
kernel size=3	13.90	0.54	113.89	74.41	5.24	32.07	0.937
kernel size=7	14.47	<b>0.56</b>	108.75	70.55	4.93	33.94	0.961
BIR-D with 5 × 5 kernel	<b>14.52</b>	<b>0.56</b>	<b>105.42</b>	<b>68.98</b>	<b>4.87</b>	<b>34.12</b>	<b>0.968</b>

Table 7: The ablation study of kernel size in blind issues.

Task	4 × Super resolution				Deblur			
	PSNR	SSIM	Consistency	FID	PSNR	SSIM	Consistency	FID
kernel size=13	24.05	0.66	6.65	39.02	26.12	0.74	41.29	3.09
kernel size=7	24.31	0.67	6.64	38.91	26.53	0.77	38.60	2.53
kernel size=11	24.36	0.69	6.50	38.07	26.79	0.79	38.52	2.44
BIR-D with 9 × 9 kernel	<b>24.58</b>	<b>0.71</b>	<b>6.32</b>	<b>37.54</b>	<b>27.14</b>	<b>0.84</b>	<b>37.86</b>	<b>2.32</b>
Task	25% Inpainting				Colorization			
	PSNR	SSIM	Consistency	FID	PSNR	SSIM	Consistency	FID
kernel size=7	29.58	0.80	6.17	18.09	20.07	0.76	39.85	42.29
kernel size=13	31.12	0.84	5.64	16.56	21.04	0.83	37.71	38.14
kernel size=11	32.91	0.86	5.41	16.17	21.57	0.85	37.69	38.01
BIR-D with 9 × 9 kernel	<b>33.59</b>	<b>0.90</b>	<b>5.18</b>	<b>15.73</b>	<b>22.09</b>	<b>0.89</b>	<b>36.12</b>	<b>36.58</b>

Table 8: The ablation study of kernel size in linear inverse problem.

be different. To explore the impact of kernel size on the quality of generated images, we conducted experiments using convolution kernels of different sizes in various types of image restoration tasks. As shown in Table 7, for blind image restoration tasks, the experiment showed that the results of a 5×5 convolution kernel perform best. For linear inverse tasks (Table 8), the optimal convolution kernel size was 9×9.

## G The Parameter Variations of the Optimizable Mask in the Reverse Steps

In order to visualize the variation of the parameters of convolution kernel mask in the reverse process, we conducted experiments on the test set of the LOL dataset from the low-light enhancement task. As shown in Figure 15, the mask has successfully captured certain intricate details within the low-light images, thereby facilitating the restoration of brightness during the reverse step.

## H More Blind Image Restoration Results

In this section, we present more generated results for several types of image restoration tasks in blind issues, including low-light enhancement, motion blur reduction, and HDR image restoration.

For the blind face restoration task, we randomly selected 1000 images from the LFW [14] and WIDER [15] test sets as input samples. More image results are shown in Figure 16. BIR-D effectively eliminates the blurring in degraded images, resulting in clearer and more detailed facial images.

For the low-light enhancement task, we use datasets including LOL [22] and VE-LOL-L [23]. The image results are shown in Figure 17. BIR-D achieved excellent results on different datasets, with the brightness of the generated images very close to the ground truth without losing any details during the restoration process.

For the motion blur reduction task, the datasets used include GoPro dataset [30] and HIDE dataset [31]. Figure 18 shows the results of BIR-D in eliminating motion blur. This also demonstrates the capabilities of BIR-D for unknown degradation functions.

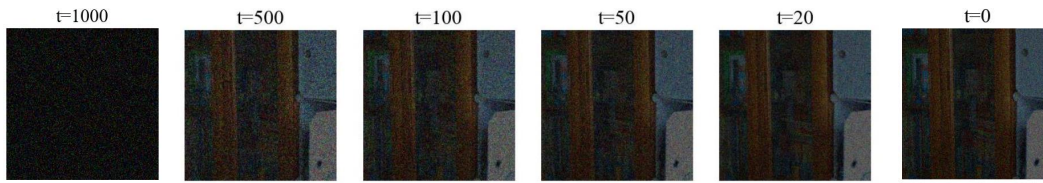


Figure 15: The changing of degradation mask during the sampling process in low light enhancement.

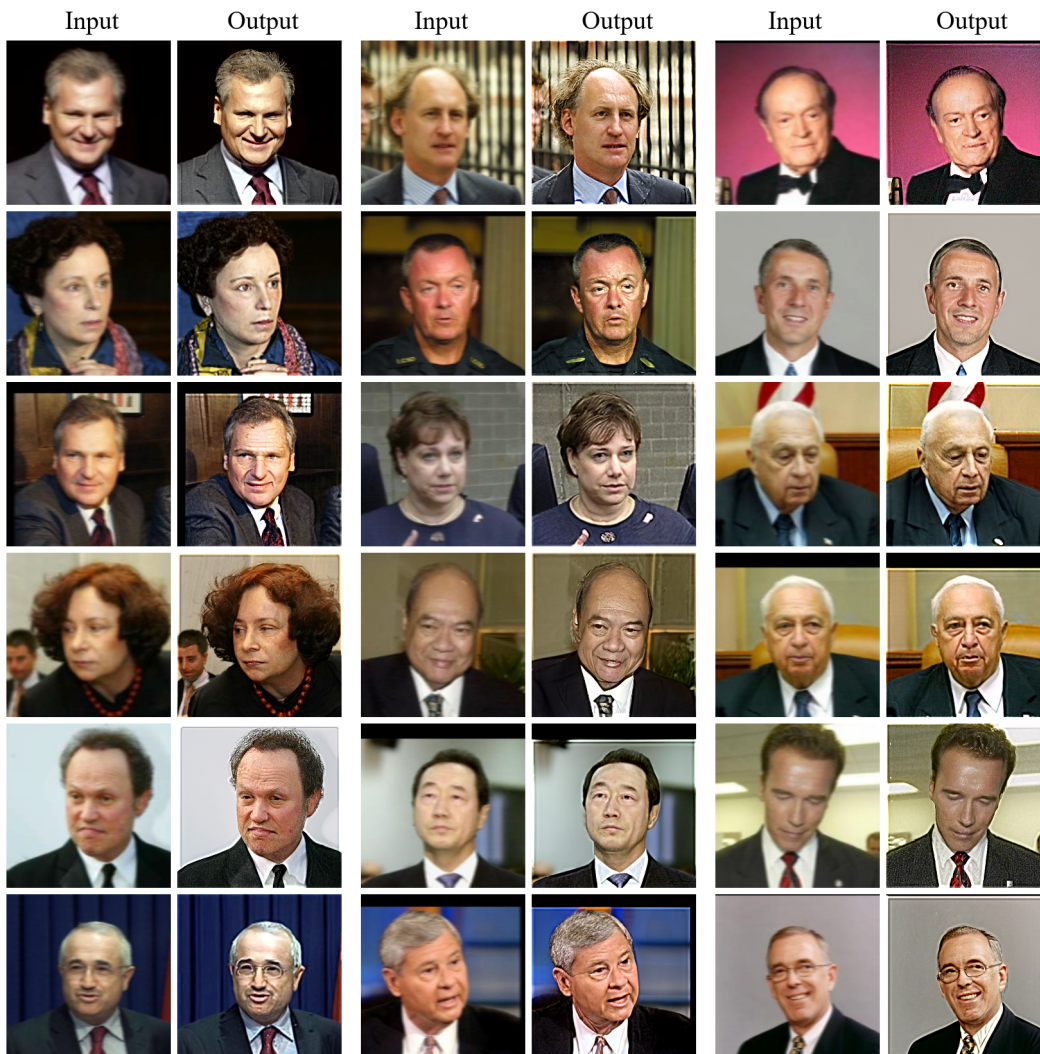


Figure 16: More image generation results for blind face restoration task. Each row consists of three sets of images, with the left and right images representing blurred facial images and BIR-D output images, respectively.

Meanwhile, we use the NTIRE2021 Multi-Frame HDR Challenge dataset [29] to test the HDR image restoration capability of BIR-D. Each image scene contains three LDR images, including long, medium, and short exposures. Following [10], we leverage three images as condition for HDR recovery. The more generated results of this task are shown in Figure 19. The over-exposure part in the image has been corrected, while the low-light part has been enhanced in brightness, resulting in a more distinct and detailed generation result.

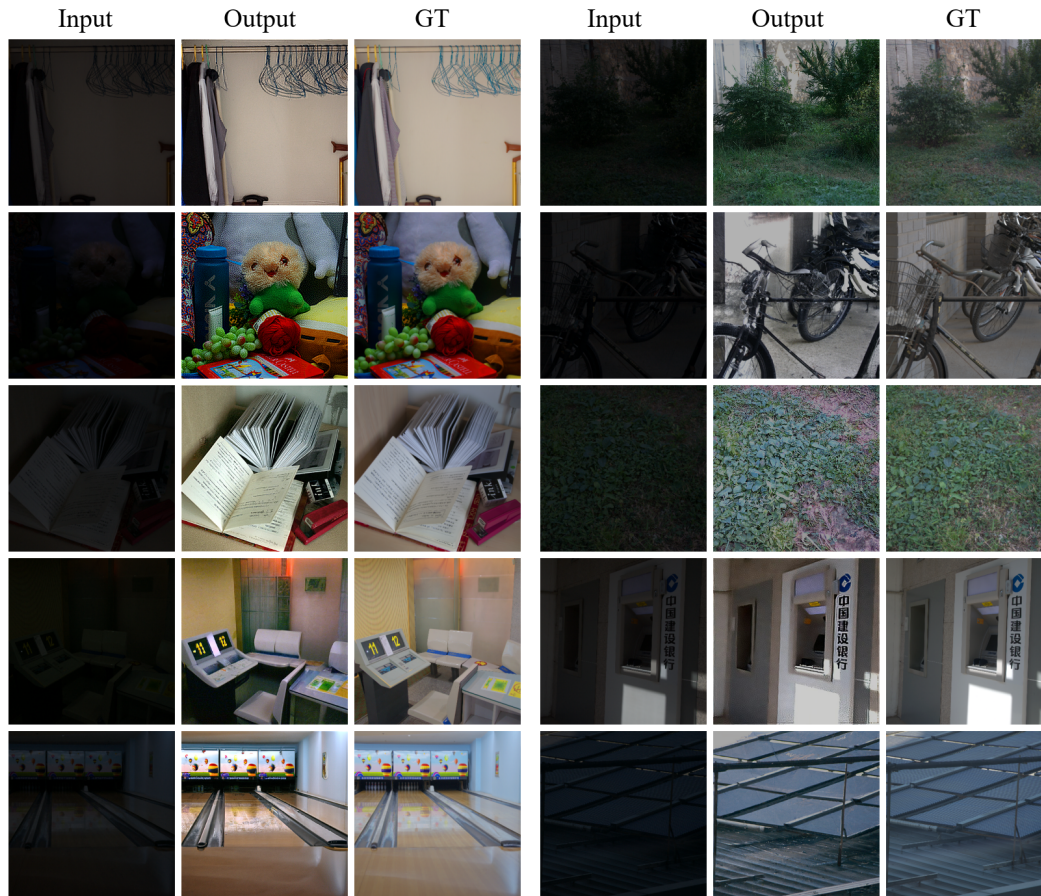


Figure 17: More image generation results for low-light enhancement task. The left half shows the image restoration results of the LOL dataset, and the right half shows the image restoration results of the VE-LOL dataset. The left, middle, and right of each group of images represent the input, BIR-D output, and ground truth respectively.

## I More Results on Commonly-used Tasks

In this section, we will provide more image restoration results on commonly used tasks, including super-resolution, colorization, deblurring, and inpainting tasks. Noted that although BIR-D has the capability to perform image restoration when the diffusion function is unknown, in order to ensure a fair comparison with other methods, an initially set and known degradation function will be used, and all image generation results and comparison metrics will be obtained under this condition. The images used in the test are all from the ImageNet dataset, and the degradation method and parameters of the input images are the same as the state-of-the-art methods, including DGP [18], SNIPS [20], DDRM [11], GDP [10], which ensures the effectiveness and fairness of the comparison.

As shown in Figure 20, BIR-D effectively removes the blur in the input image and effectively restores the details in the image. For the inpainting task, we set 25% of pixels in images to have missing pixel values, and use this as a degraded image to test the image restoration ability of BIR-D. Figure 21 shows that BIR-D has the ability to restore these 25% of missing pixels, resulting in an overall output image that is closer to the ground truth. Meanwhile, we set the ratio to 4 in the super-resolution task. As shown in Figure 22, low-resolution images can be restored from BIR-D to high-resolution images without losing clarity, while preserving various subtle details of natural images. Besides, for a given grayscale image, Figure 23 shows the level of color restoration by BIR-D for the image, and the output results also indicate the ability of BIR-D to solve the colorization task.

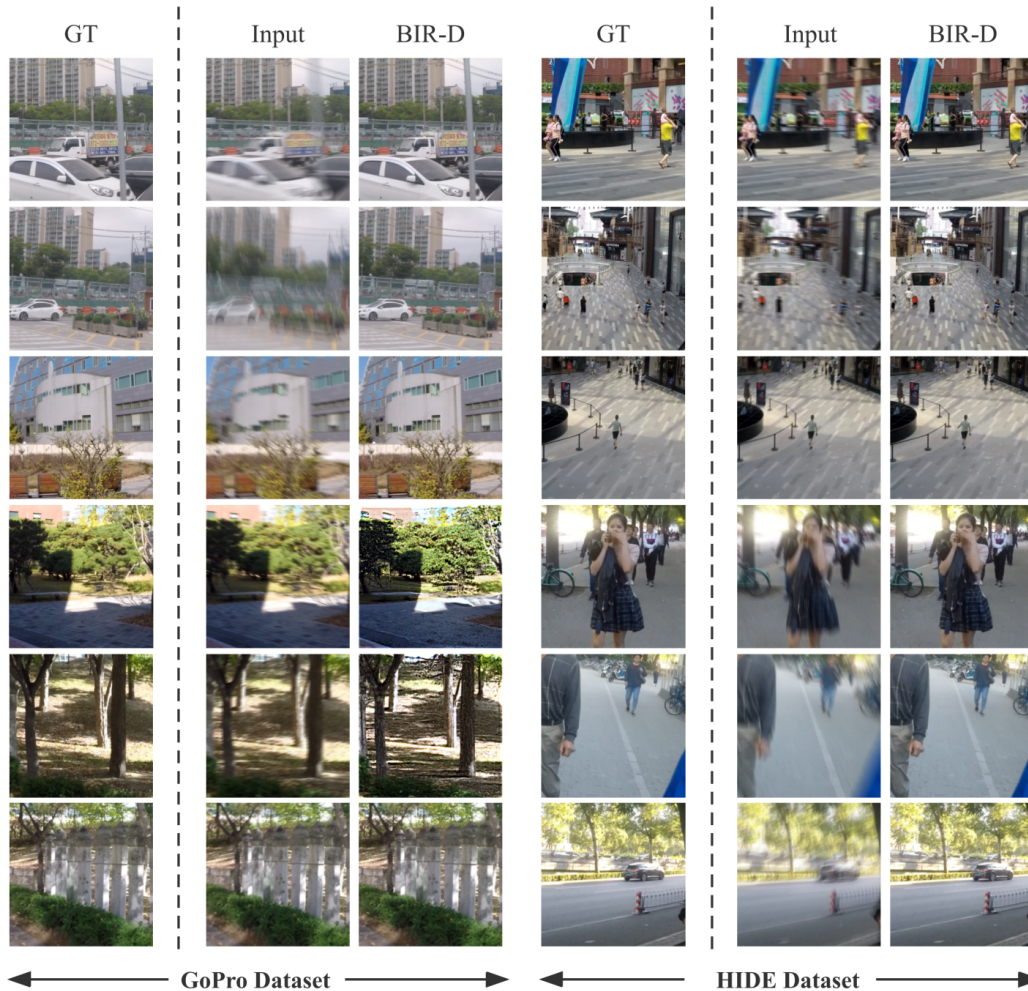


Figure 18: More image restoration results of motion blur reduction task on GoPro dataset and HIDE dataset.

## J Limitation and Future Works

Since we utilize a single pre-trained unconditional diffusion model provided by [13], the generation speed will increase when dealing with image size increasing due to the patch-based solution. In the future, it is a very promising direction to use stable diffusion to achieve faster speed in large-size image restoration.

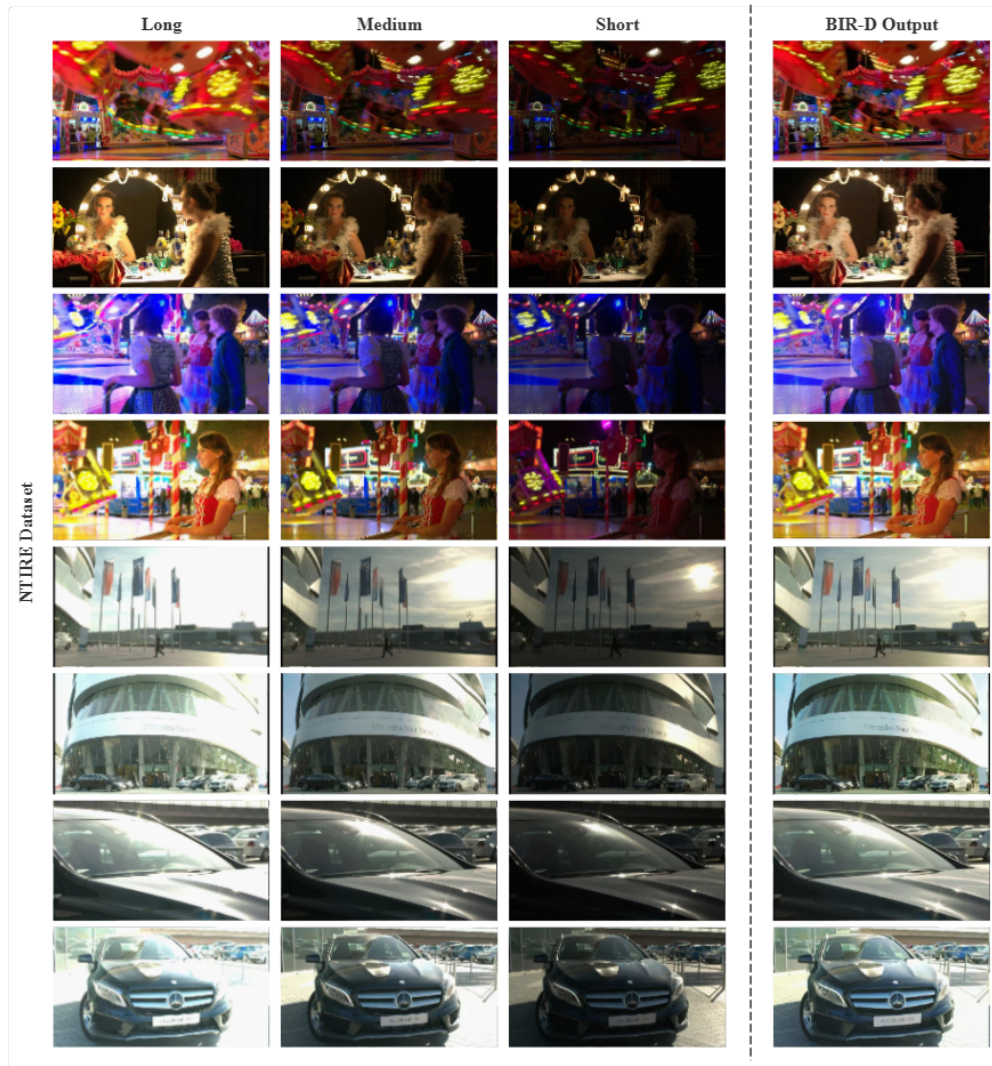


Figure 19: More image restoration results of HDR image recovery task on NTIRE2021 Multi-Frame HDR Challenge dataset.

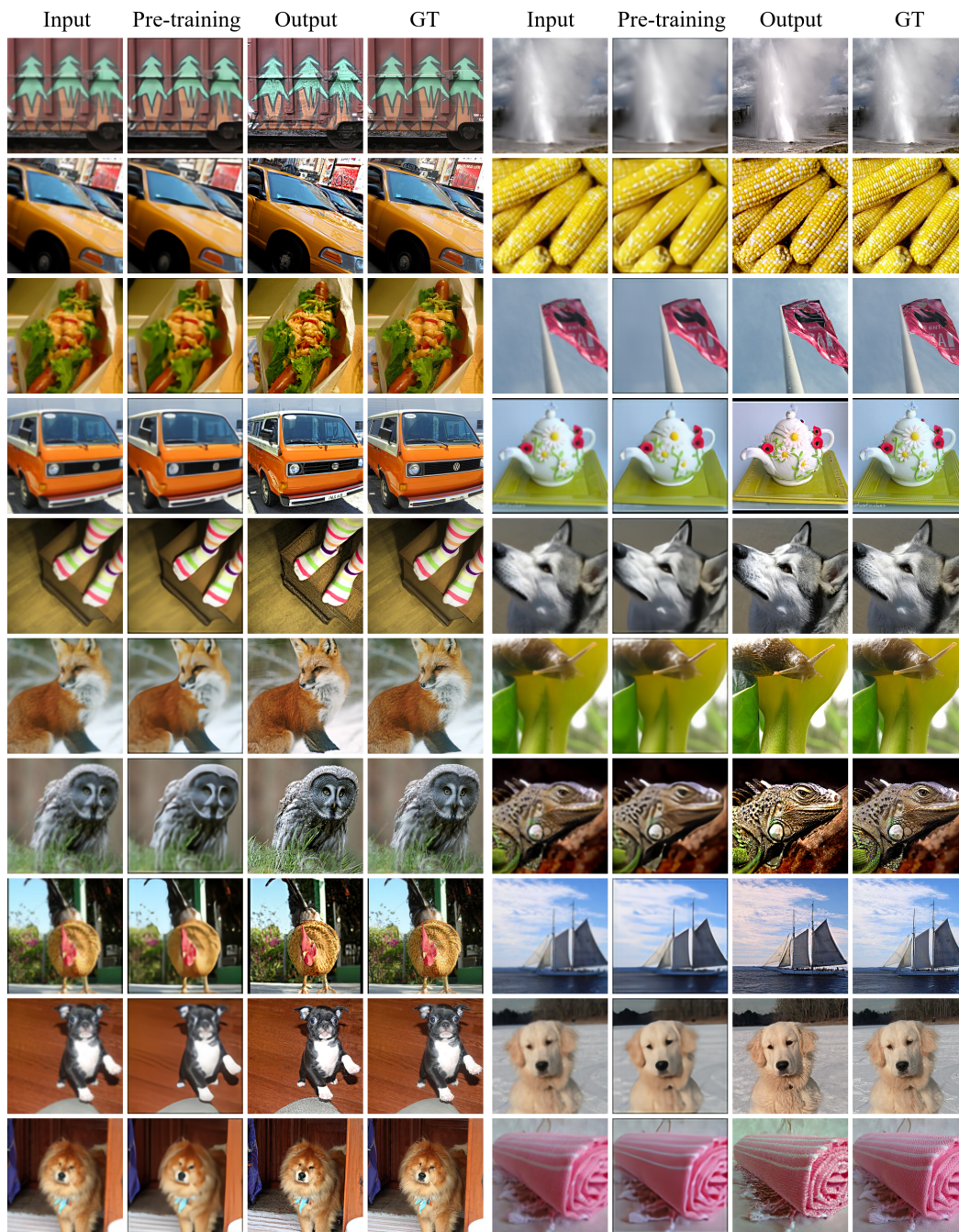


Figure 20: The image generation result of the deblurring task, where each horizontal row is composed of two sets of images, each set of images representing the input image, the image after pre-training model, the output image of BIR-D, and the ground truth from left to right.

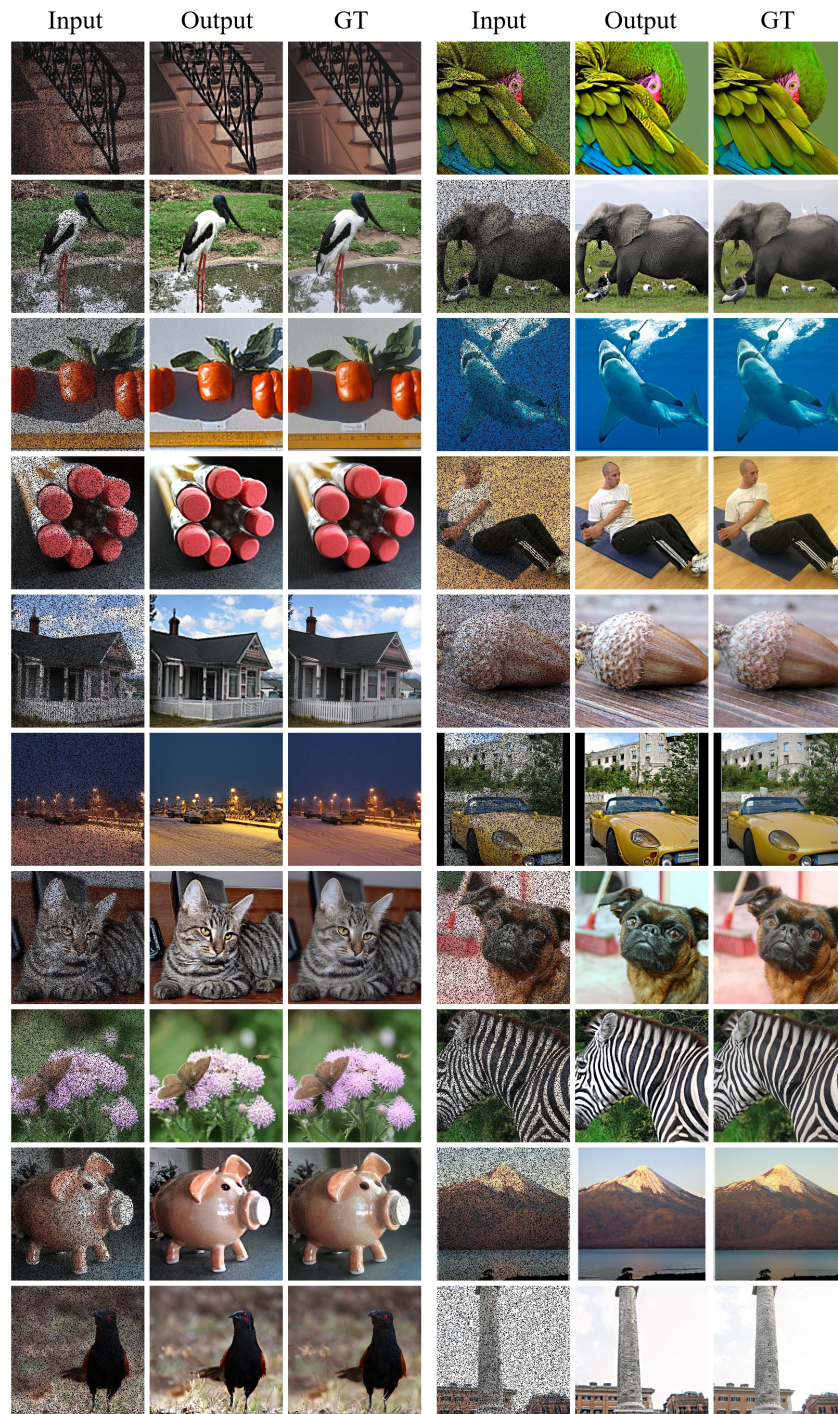


Figure 21: The image generation result of the inpainting task, where each row is composed of two sets of images and the left, middle, and right images of each set represents the degraded image, the output image of BIR-D, and the ground truth, respectively.

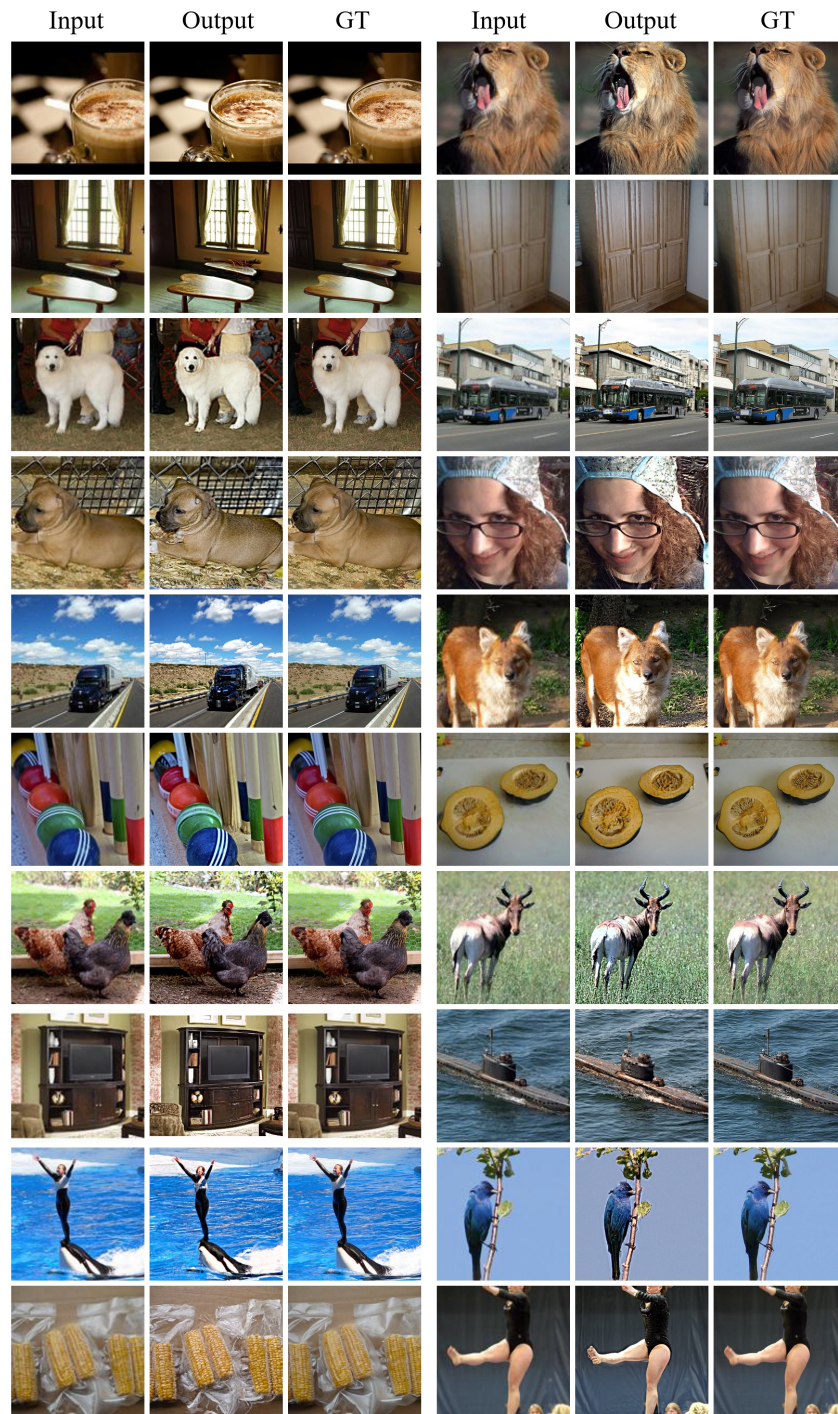


Figure 22: The image generation result of the  $4 \times$  super-resolution task, the left, middle, and right images of each set represent the low-resolution images processed by the resize function, the output images of BIR-D and the ground truth respectively.

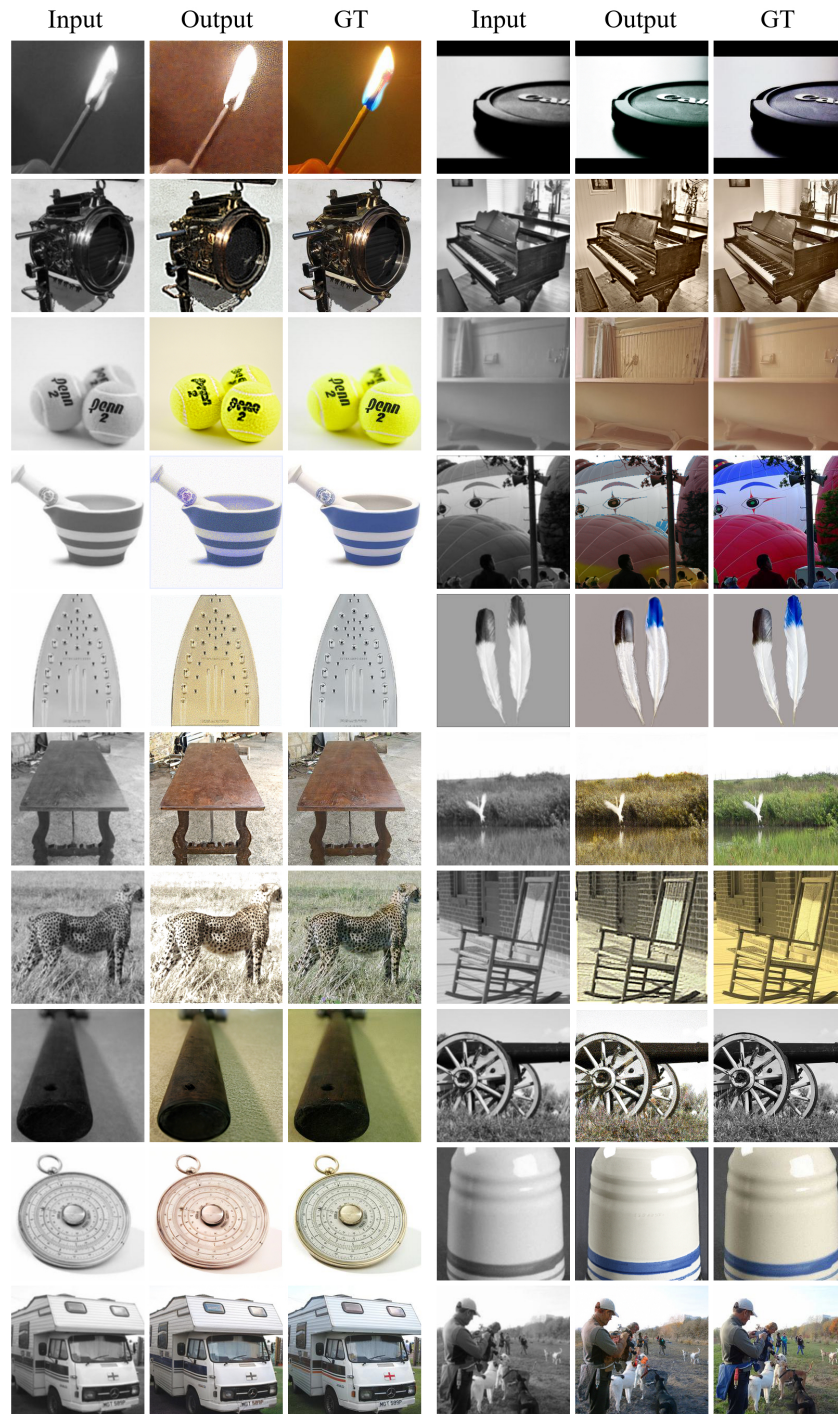


Figure 23: The image generation result of the colorization task, the left, middle and right images of each set represent the grayscale images, the output images of BIR-D and the ground truth respectively.

## NeurIPS Paper Checklist

### 1. Claims

Question: Do the main claims made in the abstract and introduction accurately reflect the paper's contributions and scope?

Answer: [Yes]

Justification: The abstract provides an overview of the main content of the paper and the introduction summarizes three contributions of the paper, which have been experimentally proven to have ideal effects.

Guidelines:

- The answer NA means that the abstract and introduction do not include the claims made in the paper.
- The abstract and/or introduction should clearly state the claims made, including the contributions made in the paper and important assumptions and limitations. A No or NA answer to this question will not be perceived well by the reviewers.
- The claims made should match theoretical and experimental results, and reflect how much the results can be expected to generalize to other settings.
- It is fine to include aspirational goals as motivation as long as it is clear that these goals are not attained by the paper.

### 2. Limitations

Question: Does the paper discuss the limitations of the work performed by the authors?

Answer: [Yes]

Justification: The discussion on limitations in the paper has been placed in the appendix.

Guidelines:

- The answer NA means that the paper has no limitation while the answer No means that the paper has limitations, but those are not discussed in the paper.
- The authors are encouraged to create a separate "Limitations" section in their paper.
- The paper should point out any strong assumptions and how robust the results are to violations of these assumptions (e.g., independence assumptions, noiseless settings, model well-specification, asymptotic approximations only holding locally). The authors should reflect on how these assumptions might be violated in practice and what the implications would be.
- The authors should reflect on the scope of the claims made, e.g., if the approach was only tested on a few datasets or with a few runs. In general, empirical results often depend on implicit assumptions, which should be articulated.
- The authors should reflect on the factors that influence the performance of the approach. For example, a facial recognition algorithm may perform poorly when image resolution is low or images are taken in low lighting. Or a speech-to-text system might not be used reliably to provide closed captions for online lectures because it fails to handle technical jargon.
- The authors should discuss the computational efficiency of the proposed algorithms and how they scale with dataset size.
- If applicable, the authors should discuss possible limitations of their approach to address problems of privacy and fairness.
- While the authors might fear that complete honesty about limitations might be used by reviewers as grounds for rejection, a worse outcome might be that reviewers discover limitations that aren't acknowledged in the paper. The authors should use their best judgment and recognize that individual actions in favor of transparency play an important role in developing norms that preserve the integrity of the community. Reviewers will be specifically instructed to not penalize honesty concerning limitations.

### 3. Theory Assumptions and Proofs

Question: For each theoretical result, does the paper provide the full set of assumptions and a complete (and correct) proof?

Answer: [Yes]

Justification: The main text of the paper provides a relatively complete proof process for the empirical formula of the guidance scale, and further supplements the proof process in the appendix.

Guidelines:

- The answer NA means that the paper does not include theoretical results.
- All the theorems, formulas, and proofs in the paper should be numbered and cross-referenced.
- All assumptions should be clearly stated or referenced in the statement of any theorems.
- The proofs can either appear in the main paper or the supplemental material, but if they appear in the supplemental material, the authors are encouraged to provide a short proof sketch to provide intuition.
- Inversely, any informal proof provided in the core of the paper should be complemented by formal proofs provided in appendix or supplemental material.
- Theorems and Lemmas that the proof relies upon should be properly referenced.

#### 4. Experimental Result Reproducibility

Question: Does the paper fully disclose all the information needed to reproduce the main experimental results of the paper to the extent that it affects the main claims and/or conclusions of the paper (regardless of whether the code and data are provided or not)?

Answer: [Yes]

Justification: The code provides all the information required to replicate the experimental results and provides instructions and guidance on how to replicate the experimental results.

Guidelines:

- The answer NA means that the paper does not include experiments.
- If the paper includes experiments, a No answer to this question will not be perceived well by the reviewers: Making the paper reproducible is important, regardless of whether the code and data are provided or not.
- If the contribution is a dataset and/or model, the authors should describe the steps taken to make their results reproducible or verifiable.
- Depending on the contribution, reproducibility can be accomplished in various ways. For example, if the contribution is a novel architecture, describing the architecture fully might suffice, or if the contribution is a specific model and empirical evaluation, it may be necessary to either make it possible for others to replicate the model with the same dataset, or provide access to the model. In general, releasing code and data is often one good way to accomplish this, but reproducibility can also be provided via detailed instructions for how to replicate the results, access to a hosted model (e.g., in the case of a large language model), releasing of a model checkpoint, or other means that are appropriate to the research performed.
- While NeurIPS does not require releasing code, the conference does require all submissions to provide some reasonable avenue for reproducibility, which may depend on the nature of the contribution. For example
  - (a) If the contribution is primarily a new algorithm, the paper should make it clear how to reproduce that algorithm.
  - (b) If the contribution is primarily a new model architecture, the paper should describe the architecture clearly and fully.
  - (c) If the contribution is a new model (e.g., a large language model), then there should either be a way to access this model for reproducing the results or a way to reproduce the model (e.g., with an open-source dataset or instructions for how to construct the dataset).
  - (d) We recognize that reproducibility may be tricky in some cases, in which case authors are welcome to describe the particular way they provide for reproducibility. In the case of closed-source models, it may be that access to the model is limited in some way (e.g., to registered users), but it should be possible for other researchers to have some path to reproducing or verifying the results.

## 5. Open access to data and code

Question: Does the paper provide open access to the data and code, with sufficient instructions to faithfully reproduce the main experimental results, as described in supplemental material?

Answer: [Yes]

Justification: The paper will include the complete code used for conducting the experiment.

Guidelines:

- The answer NA means that paper does not include experiments requiring code.
- Please see the NeurIPS code and data submission guidelines (<https://nips.cc/public/guides/CodeSubmissionPolicy>) for more details.
- While we encourage the release of code and data, we understand that this might not be possible, so “No” is an acceptable answer. Papers cannot be rejected simply for not including code, unless this is central to the contribution (e.g., for a new open-source benchmark).
- The instructions should contain the exact command and environment needed to run to reproduce the results. See the NeurIPS code and data submission guidelines (<https://nips.cc/public/guides/CodeSubmissionPolicy>) for more details.
- The authors should provide instructions on data access and preparation, including how to access the raw data, preprocessed data, intermediate data, and generated data, etc.
- The authors should provide scripts to reproduce all experimental results for the new proposed method and baselines. If only a subset of experiments are reproducible, they should state which ones are omitted from the script and why.
- At submission time, to preserve anonymity, the authors should release anonymized versions (if applicable).
- Providing as much information as possible in supplemental material (appended to the paper) is recommended, but including URLs to data and code is permitted.

## 6. Experimental Setting/Details

Question: Does the paper specify all the training and test details (e.g., data splits, hyper-parameters, how they were chosen, type of optimizer, etc.) necessary to understand the results?

Answer: [Yes]

Justification: The experimental section of the paper provides information such as the dataset used and the size of the convolution kernel. The complete detailed information is provided in the appendix and code.

Guidelines:

- The answer NA means that the paper does not include experiments.
- The experimental setting should be presented in the core of the paper to a level of detail that is necessary to appreciate the results and make sense of them.
- The full details can be provided either with the code, in appendix, or as supplemental material.

## 7. Experiment Statistical Significance

Question: Does the paper report error bars suitably and correctly defined or other appropriate information about the statistical significance of the experiments?

Answer: [Yes]

Justification: The blind image restoration model constructed in the paper has the randomness of image generation, and information such as the sources of errors and the variability factors controlling errors are placed in the appendix.

Guidelines:

- The answer NA means that the paper does not include experiments.
- The authors should answer "Yes" if the results are accompanied by error bars, confidence intervals, or statistical significance tests, at least for the experiments that support the main claims of the paper.

- The factors of variability that the error bars are capturing should be clearly stated (for example, train/test split, initialization, random drawing of some parameter, or overall run with given experimental conditions).
- The method for calculating the error bars should be explained (closed form formula, call to a library function, bootstrap, etc.)
- The assumptions made should be given (e.g., Normally distributed errors).
- It should be clear whether the error bar is the standard deviation or the standard error of the mean.
- It is OK to report 1-sigma error bars, but one should state it. The authors should preferably report a 2-sigma error bar than state that they have a 96% CI, if the hypothesis of Normality of errors is not verified.
- For asymmetric distributions, the authors should be careful not to show in tables or figures symmetric error bars that would yield results that are out of range (e.g. negative error rates).
- If error bars are reported in tables or plots, The authors should explain in the text how they were calculated and reference the corresponding figures or tables in the text.

## 8. Experiments Compute Resources

Question: For each experiment, does the paper provide sufficient information on the computer resources (type of compute workers, memory, time of execution) needed to reproduce the experiments?

Answer: [Yes]

Justification: The detailed information about the experiment in the paper is introduced in the appendix and code.

Guidelines:

- The answer NA means that the paper does not include experiments.
- The paper should indicate the type of compute workers CPU or GPU, internal cluster, or cloud provider, including relevant memory and storage.
- The paper should provide the amount of compute required for each of the individual experimental runs as well as estimate the total compute.
- The paper should disclose whether the full research project required more compute than the experiments reported in the paper (e.g., preliminary or failed experiments that didn't make it into the paper).

## 9. Code Of Ethics

Question: Does the research conducted in the paper conform, in every respect, with the NeurIPS Code of Ethics <https://neurips.cc/public/EthicsGuidelines>?

Answer: [Yes]

Justification: The research conducted in the paper conforms to the NeuroIPS Code of Ethics in all aspects

Guidelines:

- The answer NA means that the authors have not reviewed the NeurIPS Code of Ethics.
- If the authors answer No, they should explain the special circumstances that require a deviation from the Code of Ethics.
- The authors should make sure to preserve anonymity (e.g., if there is a special consideration due to laws or regulations in their jurisdiction).

## 10. Broader Impacts

Question: Does the paper discuss both potential positive societal impacts and negative societal impacts of the work performed?

Answer: [N/A]

Justification: There is no societal impact of the work performed.

Guidelines:

- The answer NA means that there is no societal impact of the work performed.

- If the authors answer NA or No, they should explain why their work has no societal impact or why the paper does not address societal impact.
- Examples of negative societal impacts include potential malicious or unintended uses (e.g., disinformation, generating fake profiles, surveillance), fairness considerations (e.g., deployment of technologies that could make decisions that unfairly impact specific groups), privacy considerations, and security considerations.
- The conference expects that many papers will be foundational research and not tied to particular applications, let alone deployments. However, if there is a direct path to any negative applications, the authors should point it out. For example, it is legitimate to point out that an improvement in the quality of generative models could be used to generate deepfakes for disinformation. On the other hand, it is not needed to point out that a generic algorithm for optimizing neural networks could enable people to train models that generate Deepfakes faster.
- The authors should consider possible harms that could arise when the technology is being used as intended and functioning correctly, harms that could arise when the technology is being used as intended but gives incorrect results, and harms following from (intentional or unintentional) misuse of the technology.
- If there are negative societal impacts, the authors could also discuss possible mitigation strategies (e.g., gated release of models, providing defenses in addition to attacks, mechanisms for monitoring misuse, mechanisms to monitor how a system learns from feedback over time, improving the efficiency and accessibility of ML).

#### 11. Safeguards

Question: Does the paper describe safeguards that have been put in place for responsible release of data or models that have a high risk for misuse (e.g., pretrained language models, image generators, or scraped datasets)?

Answer: [No]

Justification: This paper poses no such risks.

Guidelines:

- The answer NA means that the paper poses no such risks.
- Released models that have a high risk for misuse or dual-use should be released with necessary safeguards to allow for controlled use of the model, for example by requiring that users adhere to usage guidelines or restrictions to access the model or implementing safety filters.
- Datasets that have been scraped from the Internet could pose safety risks. The authors should describe how they avoided releasing unsafe images.
- We recognize that providing effective safeguards is challenging, and many papers do not require this, but we encourage authors to take this into account and make a best faith effort.

#### 12. Licenses for existing assets

Question: Are the creators or original owners of assets (e.g., code, data, models), used in the paper, properly credited and are the license and terms of use explicitly mentioned and properly respected?

Answer: [Yes]

Justification: The original papers used in the article have been cited and annotated with their sources.

Guidelines:

- The answer NA means that the paper does not use existing assets.
- The authors should cite the original paper that produced the code package or dataset.
- The authors should state which version of the asset is used and, if possible, include a URL.
- The name of the license (e.g., CC-BY 4.0) should be included for each asset.
- For scraped data from a particular source (e.g., website), the copyright and terms of service of that source should be provided.

- If assets are released, the license, copyright information, and terms of use in the package should be provided. For popular datasets, [paperswithcode.com/datasets](https://paperswithcode.com/datasets) has curated licenses for some datasets. Their licensing guide can help determine the license of a dataset.
- For existing datasets that are re-packaged, both the original license and the license of the derived asset (if it has changed) should be provided.
- If this information is not available online, the authors are encouraged to reach out to the asset's creators.

### 13. **New Assets**

Question: Are new assets introduced in the paper well documented and is the documentation provided alongside the assets?

Answer: [Yes]

Justification: The assets introduced in the paper are all submitted after being documented.

Guidelines:

- The answer NA means that the paper does not release new assets.
- Researchers should communicate the details of the dataset/code/model as part of their submissions via structured templates. This includes details about training, license, limitations, etc.
- The paper should discuss whether and how consent was obtained from people whose asset is used.
- At submission time, remember to anonymize your assets (if applicable). You can either create an anonymized URL or include an anonymized zip file.

### 14. **Crowdsourcing and Research with Human Subjects**

Question: For crowdsourcing experiments and research with human subjects, does the paper include the full text of instructions given to participants and screenshots, if applicable, as well as details about compensation (if any)?

Answer: [N/A]

Justification: The paper does not involve crowdsourcing nor research with human subjects.

Guidelines:

- The answer NA means that the paper does not involve crowdsourcing nor research with human subjects.
- Including this information in the supplemental material is fine, but if the main contribution of the paper involves human subjects, then as much detail as possible should be included in the main paper.
- According to the NeurIPS Code of Ethics, workers involved in data collection, curation, or other labor should be paid at least the minimum wage in the country of the data collector.

### 15. **Institutional Review Board (IRB) Approvals or Equivalent for Research with Human Subjects**

Question: Does the paper describe potential risks incurred by study participants, whether such risks were disclosed to the subjects, and whether Institutional Review Board (IRB) approvals (or an equivalent approval/review based on the requirements of your country or institution) were obtained?

Answer: [N/A]

Justification: The paper does not involve crowdsourcing nor research with human subjects.

Guidelines:

- The answer NA means that the paper does not involve crowdsourcing nor research with human subjects.
- Depending on the country in which research is conducted, IRB approval (or equivalent) may be required for any human subjects research. If you obtained IRB approval, you should clearly state this in the paper.

- We recognize that the procedures for this may vary significantly between institutions and locations, and we expect authors to adhere to the NeurIPS Code of Ethics and the guidelines for their institution.
- For initial submissions, do not include any information that would break anonymity (if applicable), such as the institution conducting the review.